Katharina Weingrill, B.Eng.

Modelling of the Isolation Resistance
of a PEM Fuel Cell System

MASTER'S THESIS

to achieve the university degree of

Master of Science

Master's degree programme:

Environmental System Sciences / Climate Change and Environmental Technology

submitted to

Graz University of Technology

Supervisor

Ass.Prof. Dipl.-Ing. Dr.techn. Katrin Friedl

Institute of Electrical Power Systems

Co-Supervisor

Dipl.-Ing. Carina Lehmal

Graz, July 2024

IFEAN

© fotopro -

Modelling of the Isolation Resistance of a PEM Fuel Cell System

A Master Thesis by
Katharina Weingrill, B.Eng.

Supervisor
Katrin Friedl, Ass.Prof. Dipl.-Ing. Dr.techn.

Co-Supervisor
Carina Lehmal, Dipl.-Ing.

July 2024

Graz University of Technology
Institute of Electric Power Systems
Inffeldgasse 18/I
8010 Graz
Austria

Head of Institute
Robert Schürhuber, Univ.-Prof. DDI Dr.

Supervisor
Katrin Friedl, Ass.Prof. Dipl.-Ing. Dr.techn.

Co-Supervisor
Carina Lehmal, Dipl.-Ing.

A Master Thesis by
Katharina Weingrill, B.Eng.

July 2024

Statutory Declaration

I declare that I have authored this thesis independently, that I have not used other than the declared sources / resources, and that I have explicitly marked all material which has been quoted either literally or by content from the used sources.

Graz, 29th July 2024

Katharina Weingrill

Acknowledgements

Abstract

The European CO_2 emission standards, most recently the Euro 7, create the urge for an increased number of zero emission vehicles on the road. Polymer electrolyte membrane (PEM) fuel cell electric vehicles (FCEV) represent one of such zero emission solutions, especially attractive for heavy duty vehicles. For such high power applications it is often necessary to connect two or more fuel cell systems in parallel, which makes the legally required isolation resistance according to ISO6469-3 a critical parameter. This thesis aims to create a model of the isolation resistance of a PEM fuel cell system for the estimation of the system's isolation resistance, especially in an early design stage. The following research questions are addressed: "What possibilities are there to improve the isolation resistance of a PEM fuel cell system?" and "How can the isolation resistance of a PEM fuel cell system be modelled?" Both research questions are answered by first establishing the technical links and second by validating the outcome with experimental data. The required data is gathered from the AVL Fuel Cell Demo Truck 156 kW PEM fuel cell system. The model is set up in Excel with the basic element being a network of serial and parallel resistance segments modeling the coolant path of the fuel cell system. The offset between measurement data and modeled data is up to 20 %, from which 12.5 % is linked to a load dependent conductivity change across the stack. The model output has a negative offset, which is favorable to guarantee compliance. Measures to optimize the isolation resistance of the first design stage of the fuel cell system for the Demo Truck are suggested and modelled to quantify their effects.

Kurzfassung

Die europäischen CO2-Emissionsnormen, zuletzt die Euro-7-Norm, führen dazu, dass immer mehr emissionsfreie Fahrzeuge auf die Straße kommen. Brennstoffzellenfahrzeuge mit Polymerelektrolytmembran (PEM) sind eine dieser emissionsfreien Lösungen, die vor allem für Nutzfahrzeuge attraktiv sind. Für solche Anwendungen ist es oft notwendig, zwei oder mehr Brennstoffzellensysteme parallel zu verschalten, wobei die Isolationsanforderung gemäß ISO6469-3 ein kritischer Parameter ist. Ziel dieser Arbeit ist die Erstellung eines Modells des Isolationswiderstandes eines Brennstoffzellensystems zur Abschätzung des Isolationswiderstandes, insbesondere in einer frühen Entwurfsphase. Die folgenden Forschungsfragen werden behandelt: „Welche Möglichkeiten gibt es, den Isolationswiderstand eines PEM-Brennstoffzellensystems zu verbessern?" und „Wie kann der Isolationswiderstand eines PEM-Brennstoffzellensystems modelliert werden?" Zur Beantwortung beider Forschungsfragen werden zunächst die technischen Zusammenhänge erarbeitet und anschließend die Ergebnisse mit experimentellen Daten validiert. Die benötigten Daten werden aus dem 156 kW PEM-Brennstoffzellensystem des AVL Fuel Cell Demo Truck erfasst. Das erstellte Excel-Modell besteht grundsätzlich aus einem Netzwerk von seriellen und parallelen Widerstandssegmenten und modelliert damit den Kühlmittelpfad des Brennstoffzellensystems. Die Abweichung zwischen Messdaten und dem Modellergebnis liegt bei < 20 %, wovon 12.5 % auf eine lastabhängige Leitfähigkeitsänderung entlang des Kühlmittelsystems zurückzuführen ist. Die Modellausgabe weist einen negativen Offset auf, was vorteilhaft ist, um die Einhaltung der Anforderungen zu gewährleisten. Es werden Maßnahmen zur Optimierung des Isolationswiderstandes der ersten Entwicklungsstufe des 156 kW Brennstoffzellensystems vorgeschlagen und modelliert, um ihre Verbesserung zu quantifizieren.

List of Symbols

A	Area, cross section
E	Potential
F	Factor
I	Current
Iso_{RQ}	Electrical isolation
j	Current density
l	Length
n	Number of x
η	Efficiency
Q	Volume flow
R	Resistance
R_{iso}	Isolation resistance
t	Time, duration
V	Voltage
σ	Electrical conductivity

List of Abbreviations

AC	Alternating Current
BEV	Battery Electric Vehicles
BMS	Battery Management System
BoP	Balance of Plant components
BPP	Bipolar Plates
Cx	Coolant
DC	Direct Current
DI	Deionized
EU	European Union
FC	Fuel Cell
FCEV	Fuel Cell Electric Vehicle
HT	High Temperature
HV	High Voltage
IEV	International Electrotechnical Vocabulary
IMD	Isolation Monitoring Device
IT	Isolated Terra, unearthed system
IPCC	Intergovernmental Panel on Climate Change
LT	Low Temperature
LV	Low Voltage (12 or 24 V in automotive systems)
MEA	Membrane Electrode Assembly
OEM	Original Equipment Manufacturer
Ox	Air (Oxidant)
PEM	Polymer Electrolyte Membrane
PEMFC	Polymer Electrolyte Membrane Fuel Cell
PFSA	Perfluorosulfonic Acid
RHE	Reversible Hydrogen Electrode
RQ	Requirement
TC	Turbo Charger

Table of Contents

1 Introduction

The Paris Agreement adopted in 2015 [1] aims to limit climate change with its main objective of "Holding the increase in the global average temperature to well below 2 °C above pre-industrial levels and pursuing efforts to limit the temperature increase to 1.5 °C above pre-industrial levels, recognizing that this would significantly reduce the risks and impacts of climate change". The Intergovernmental Panel on Climate Change (IPCC) [2] further states with very high confidence:

> "Climate change is a threat to human well-being and planetary health. There is a
> rapidly closing window of opportunity to secure a liveable and sustainable future
> for all".

To limit human-caused global warming it is necessary to transition to net zero CO_2 emissions. This requires emission reduction in all sectors [2]. The European Union (EU) defines emission standards for road vehicles with the goal to reduce CO_2 emissions. For trucks and busses (heavy-duty) Euro VI [3] defines the currently applicable standards. The 2019 amendment [4] points out the following targets to reduce CO_2 emissions, compared to the 2005 reference CO_2 emissions, for new heavy-duty vehicles: (a) 15 % reduction from 2025 onwards and (b) 30 % reduction from 2030 onwards.

The successor, Euro 7 [5], will be applicable for all road vehicles from passenger cars to heavy-duty vehicles. The more stringent rules are still under discussions but will likely be applicable from 2027 onwards for heavy-duty applications.

The current and future regulations undermine the need for zero emission vehicles on the market. Polymer electrolyte membrane (PEM) fuel cell electric vehicles (FCEV) represent one of such zero emission solutions. The advantages of FCEVs compared to battery electric vehicles (BEV), being longer driving ranges and short fueling times (within minutes) [6], are especially important for heavy-duty vehicles. For high power applications it is often necessary to connect two or more fuel cell systems in parallel. Especially, if the systems are galvanically connected on the high voltage (HV) bus, the legally required isolation resistance according to ISO6469-3 [7] is a critical parameter.

In a development process, the resulting isolation resistance is mostly unknown until the system is on the testbed. Therefore, measures to increase the isolation resistance are often taken in a late stage of the system development. The possibilities then are usually limited and the costs for changes are high, resulting in considerable risks. The goal of this thesis is to reduce the risks by developing a tool to model the isolation resistance which can be applied early in the design process. A further goal is to provide a suggestion of measures to improve the isolation resistance, which can be applied if the model's output prognoses an insufficient isolation resistance.

To be concise, it is the aim of this thesis to answer the following research questions:

- What possibilities are there to improve the isolation resistance of a PEM fuel cell system?
- How can the isolation resistance of a PEM fuel cell system be modelled?

Both research questions are answered by first establishing the technical links and second by validating the outcome with experimental data. The required data is gathered from the AVL Demo Truck 156 kW PEM fuel cell system. This system is designed to be used in a modular way to fit the overall power demand. In the AVL Demo Truck project it is planned to build a truck with 42 t gross combination weight and 540 kW electrical drive power. Two fuel cell system are integrated. They shall fulfill the isolation resistance requirements without galvanic isolation from the HV bus, for which measures must be implemented from the first to the second design stage.

The first two chapters of this thesis provide background to isolation resistance and fuel cell systems in general. The second chapter also gives some insights to limitations of scaling fuel cell systems. Chapter 4 dives deeper into the ground paths of the fuel cell system, with the focus on the coolant sub system. With the knowledge provided, it is possible to answer the first research question, which will be done in chapter 5. The next chapter is dedicated to introducing the isolation resistance model, which answers the second research question. The technical links to answer the research question are already established in chapter 4.2. Chapter 7 focuses on the validation of the model with test data and the analysis of the measures implemented. The last chapter is the discussion of the results.

2 Isolation Resistance

The isolation resistance is a central element of a vehicle's electrical safety. It can be defined as [7]

> "resistance between live parts of an electric circuit and the electric chassis as well as other electric circuits which are insulated from this electric circuit"

Within the ISO 6469-3 [7] the terms isolation resistance and insulation resistance are used interchangeably. Still, both terms definitions within the International Electrotechnical Vocabulary (IEV) are given:

- **insulation** is the "part of an electrotechnical product which separates conducting parts at different electric potentials during operation or insulates such parts from the surroundings" [8]
- **isolation** describes the "disconnection providing adequate insulation between electrical equipment, a system, an installation or part of an installation and their energy sources" [9]

In other words, isolation can be described as a function fulfilled by the insulation. However, the insulation is the barrier which must proof the withstand voltage. In this study, the function is the dominant interest, which is why the term isolation resistance is used.

The electrical isolation in Ω/Volt is an expression of the current flowing through an object, as shown in equation (2-1). The relation is a form of Ω law ($V = I \cdot R$). It shows that a higher electrical isolation defined with Iso_{RQ} leads to a lower current potentially passing through the human body.

$$Iso_{\mathrm{RQ}} = \frac{R\ (Ohm)}{V\ (V)} = \frac{1}{I\ (A)} \tag{2-1}$$

Where R is the isolation resistance, V is the maximum voltage and I is the ground current.

The relevant SAE document (J2578), ISO document (ISO 6469-3 [7]) and ECE regulation (ECE/TRANS/180/Add.13) define the same thresholds: The minimum isolation resistance, divided by the working voltage, shall have a minimum value of

- 100 Ω/Volt for DC circuits, and
- 500 Ω/Volt for AC circuits

The electric traction motor as well as the fuel cell compressor are commonly AC components on the HV bus. The fuel cell itself is a DC component. Therefore, there is a combined circuit of AC and DC voltage to consider. In this case the ISO 6469-3 [7] specifies two options for the minimum value of the minimum isolation resistance, divided by the working voltage:

- Option 1: 500 Ω/V for the combined circuit, or
- Option 2: 100 Ω/V, if at least one alternative protection measure is applied to the AC circuit.

The alternative protection measures shall not only provide basic protection but also fault protection. Generally, these are either double insulation (meaning double withstand voltage, clearance and creepage distances) or protective enclosures. No further evaluation on specific alternative protection measures is done within this thesis.

2.1 Body Current and their Effects

The rationale for the minimum isolation resistance is the protection against electric shock. Electric shock is the "physiological effect resulting from an electric current passing through a human body or livestock" [9]. To understand the requirements on the isolation resistance, it is therefore necessary to investigate the critical current for the human body. The international standard for the effects on human beings and livestock is the IEC 60479-1 [10]. In Figure 2-1 and Figure 2-2 the effects of current on the human body are classified in different zones for AC and DC currents respectively. The thresholds generally depend on the area of contact, the conditions of contact (dry, wet, pressure, temperature), the path through the body and also on the physiological characteristics of the individual [10].
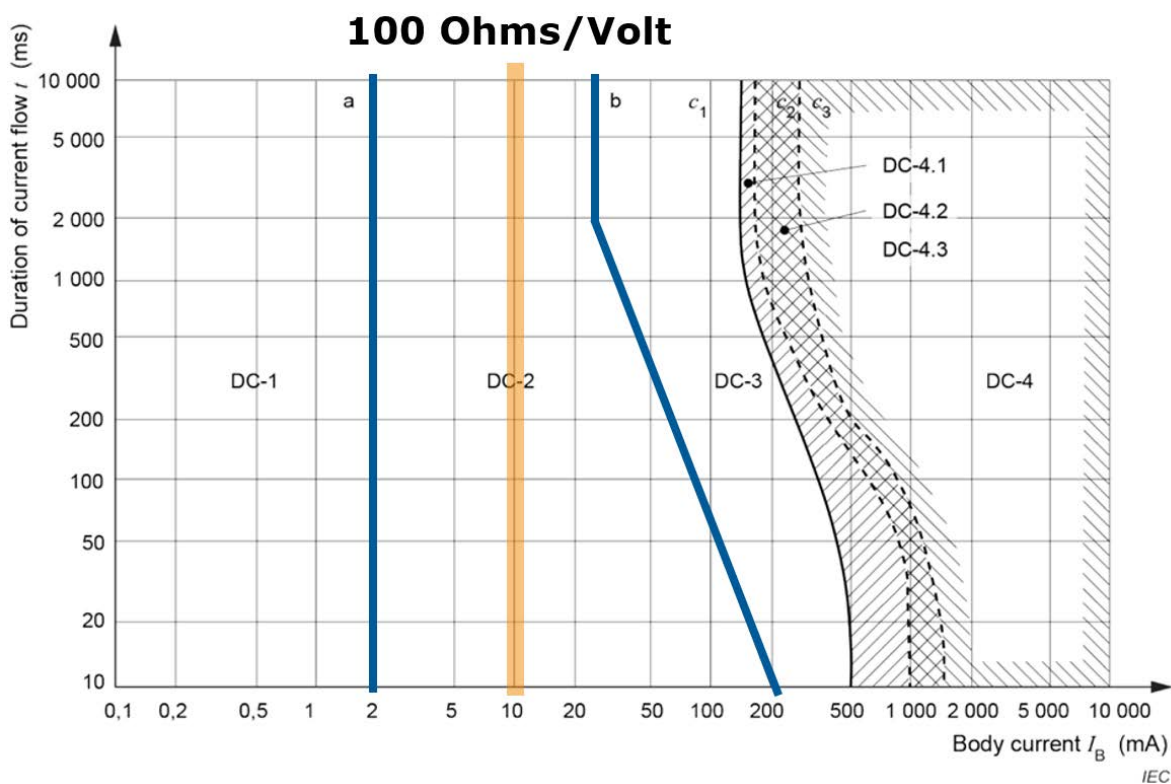
Figure 2-1: Zones of effects of DC currents on persons for a current path corresponding to left hand to feet, modified from [10]

According to equation (2-1), the values 500 Ω/Volt and 100 Ω/Volt are placed in the middle of zone AC-2 and DC-2 respectively. The effects of this range are classified as "involuntary muscular contractions likely especially when making, breaking or rapidly altering current flow but usually no harmful electrical physiological effects" [10].

The full table with the effects per zone is given in the appendix in Table 1. Briefly, in this area no harmful effects are expected. In zone AC-3 and DC-3 muscle contractions with reversible effects may happen. Above these zones, the risk of muscular fibrillation increases. [10]
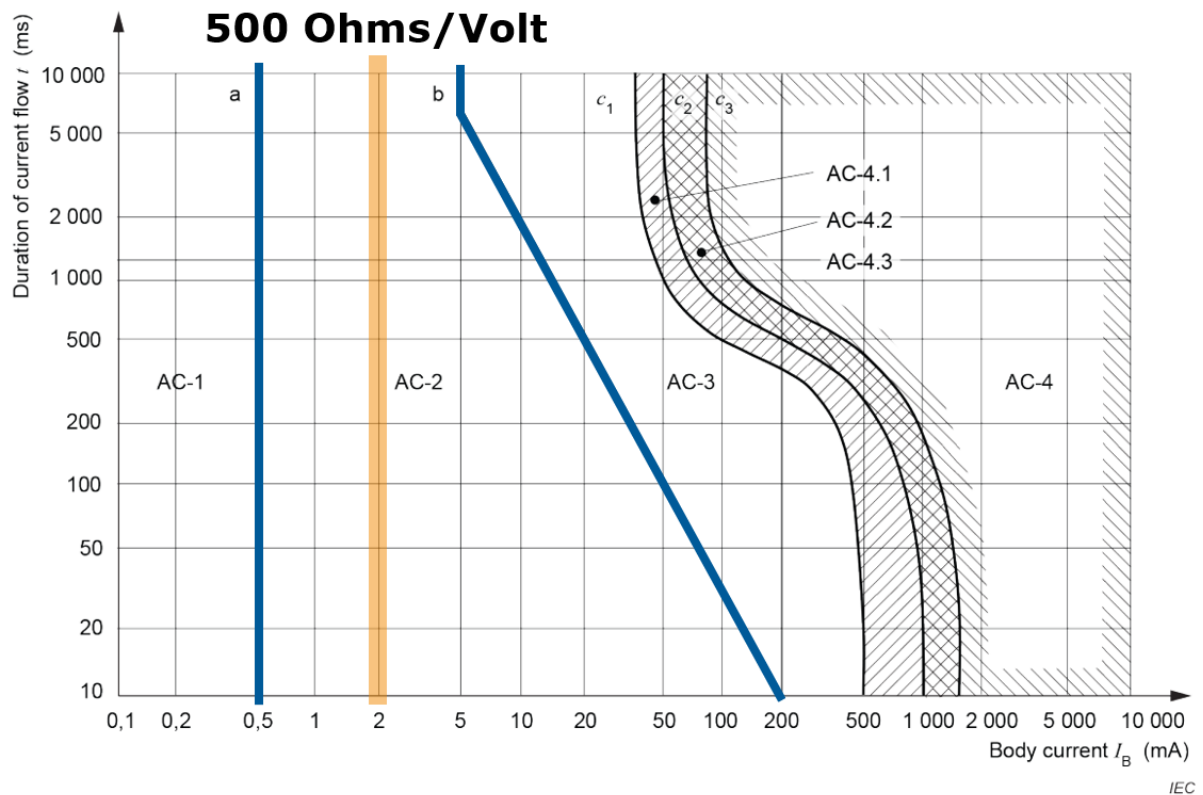
Figure 2-2: Zones of effects of AC currents (15 Hz to 100 Hz) on persons for a current path corresponding to left hand to feet, modified from [10]

Figure 2-1 and Figure 2-2 refer to the danger for currents passing from the left hand to feet. The IEC 60479-1 [10] also defines a heart-current-factor which allows a rough estimation of different current paths through the body. The equivalent body current for the given path can be calculated with the following equation:

$$I_{eq} = \frac{I_{ref}}{F}$$

(2-2)

Where

I_{ref} is the body current from the left hand to feet,

I_{eq} is the body current for the equivalent path chosen, and

F is the heart-current factor for the equivalent path chosen.

The worst-case path is chest to left hand with a factor of 1.5. That means that a current of 5 mA flowing from the left hand to feet has the same effect as a body current of 3.33 mA flowing from chest to the left hand. As the limits of 100 Ω/Volt and 500 Ω/Volt are both in the middle of their range, even by applying the factor of 1.5 there is no risk of harmful effects.

2.2 Isolation Faults in IT Systems

The majority of vehicle's HV buses are unearthed (isolated terra, IT) systems. The active parts are not connected to the vehicle's equipotential bonding. Therefore, except for high impedance connections for protection or measurement purposes, there is no intentional connection to vehicle ground. The advantage is that a single ground fault (i.e. HV+ to ground) does not cause a leakage current flow, thus, increasing the safety of the system [11]. Figure 2-3 is used to explain an IT system schematically. There is a defined voltage between HV+ and HV- which is the bus voltage V_b. The potential of chassis ground is somewhere between the potential of HV+ and HV-. The voltage between HV+ to ground is V_p and the voltage between HV- to ground is V_n. The position of the ground potential can be explained by imagining the resistances as springs. The lower the resistance, the stronger the spring is pulling the potential towards the live parts potential. In the case of Figure 2-3 the isolation resistance from HV- to ground is lower, hence pulling the potential towards it, resulting in $V_n < V_p$.

An isolation fault can also be present from HV to LV (low voltage, 12 or 24 V in automotive). As the internal resistance of the LV system, referring to the resistance of the cabling and connectors, is very small compared to the isolation resistance, it can be neglected. Therefore, it is usually sufficient to determine the isolation resistance to chassis/ground.
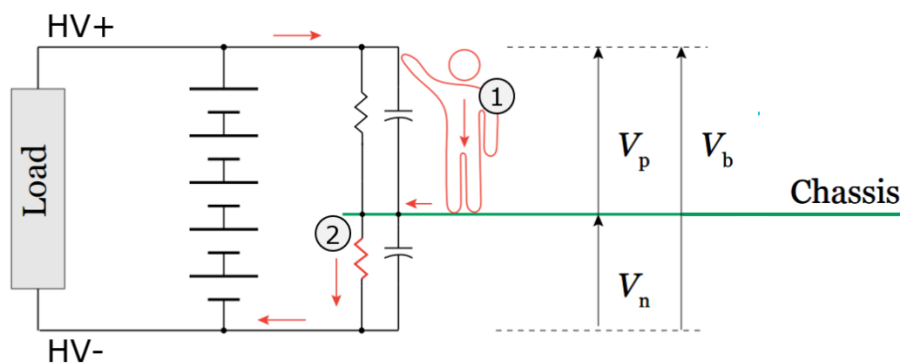
Figure 2-3: Schematic of an IT system with a double isolation fault, modified from [12]

As mentioned before, a single isolation fault does not cause a leakage current. With a single isolation fault in an HV system e.g. of a vehicle powertrain, the powertrain can continue operation, although a warning has to be displayed to the driver and the fault should be fixed as soon as possible [7]. Now, if a person touches a live part, the circuit is closed and a leakage current flows through the body. However, normally a person cannot touch live parts of the circuit, so the path through the person should not occur. That is why only in case of a double fault a dangerous electric shock according to Figure 2-1 and Figure 2-2 can occur. This case is also shown in Figure 2-3.

A double fault involves two independent faults as shown in Figure 2-3:

1) A live part of the circuit can be touched by a person, and
2) the isolation resistance is below the legal threshold (100 or 500 Ω/Volt)

Generally, isolation faults occur mainly due to faults of HV components and HV cabling such as an internal short circuit or a dielectric breakdown. In PEM fuel cell systems, however, the coolant is flowing through the stack which allows electric current to find a path through ions in the coolant to ground, thus, reducing the isolation resistance. This aspect is discussed in detail in chapter 4.2.

One can differentiate between symmetrical and unsymmetrical faults. In case of a symmetrical fault V_p and V_n will be similar while in case of an unsymmetrical fault $V_p \ll V_n$ or $V_n \ll V_p$. A fault path through the coolant of fuel cell systems is a symmetrical fault, as both the positive and the negative potential of the stack are electrically connected to the coolant.

2.3 Isolation Monitoring

An isolation monitor is a "system that periodically or continuously monitors the isolation resistance between live parts and the electric chassis" [7]. If the minimum electric isolation "cannot be maintained under all operational conditions and over the entire service life" [7] the ISO 6469-3 foresees an isolation monitoring device (IMD) to be installed in the (IT) system. Alternative protection measures instead are also permitted. These are again double insulation or protective enclosures.

The IMD is usually part of the battery management system (BMS) of electric vehicles, which also include FCEVs. The simplest methods rely exclusively on the measurement of either voltage or current and do not inject a signal. They fail to detect symmetrical faults and are therefore not used for isolation resistance monitoring in IT systems. [12]

The most common method used is the signal injection method. The principle of the method is shown in Figure 2-4. A known current i_x is injected by the isolation monitor to $HV+$ and $HV-$ alternately, which results in a voltage change ΔV for the isolation resistance from $HV+$ to chassis and a distinct ΔV for the isolation resistance from $HV-$ to chassis. [12]
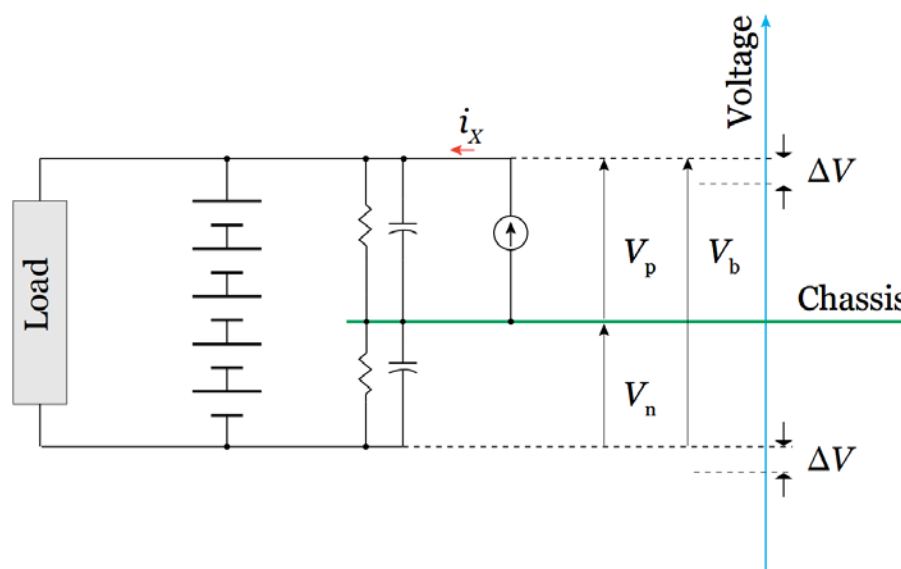
Figure 2-4: Principle of signal injection method [12]

The calculation of the isolation resistance follows again Ωs law with

$$R_{\text{iso}} = \frac{\Delta V}{I_{\text{x}}} \tag{2-3}$$

Where

R_{iso} is the isolation resistance

ΔV is the change of voltage

I_{x} is the injected current

The implementations of the signal injection method may vary by the value of the injected signal, the signal shape, the duration, etc. The Bender ISO165, an established product on the market, injects a pulsed measuring voltage and measures the current for the calculation of the isolation resistance [13].

2.4 Relevance of HV Architecture

The most common HV architecture for FCEVs is shown in Figure 2-5. As in an electric vehicle, there is a battery with a BMS and an electric motor with an inverter (DC/AC). Additional to that, the FCS is connected to the HV bus with an unidirectional boost DC/DC. Unidirectional means the energy is flowing from the fuel cell towards the HV bus only. In contrast, the energy flow of the battery is bidirectional, as the energy can flow in both directions as it is charged and discharged. Boost means that the voltage level of V_{HS} (high side) is always higher than V_{LS} (low side) when in operation. That allows a simpler converter layout.
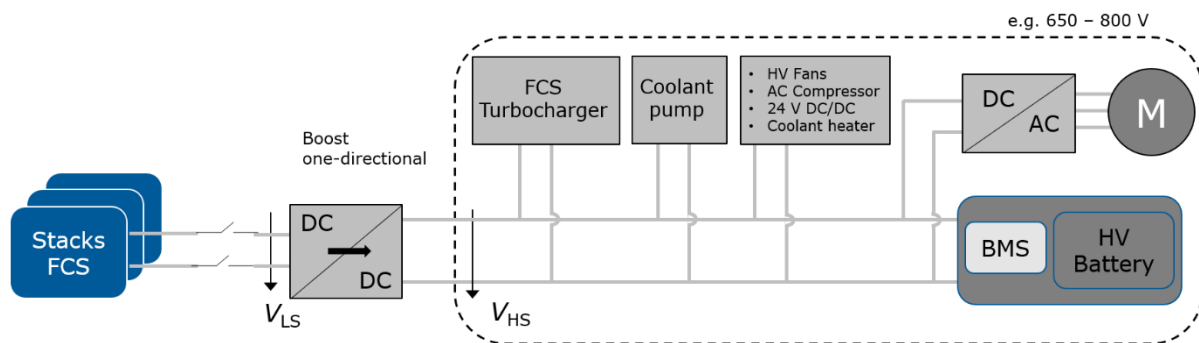
Figure 2-5: HV architecture of a FCEV with one FCS

In Figure 2-6 common cell voltages of a fuel cell for operation are shown. Details to their origin are discussed in Table 3-2 within chapter 0. The fuel cell voltage scales with the number of cells. At this point it is important that for the design of the DC/DC the operating range of the fuel cell needs to be considered. The voltage may increase up to 1.1 V/cell during the start-up of the FCS. The DC/DC does not necessarily need to convert this voltage, if the system design allows it with regards to safety and if the start up duration can be extended. The voltage will decrease on its own within a few seconds or already a small current flow of < 5 A can reduce the voltage to 0.9 V/cell within milliseconds. This is due to the current voltage characteristic of the fuel cell as will be explained in chapter 3.1 Importantly at this

point, the voltage of 1.1 V/cell should not damage the DC/DC. The lower range of 0.2 V/cell can be required for specific operating strategies during freeze start-up of a fuel cell system where losses in form of heat are ought to be maximized. A lower voltage at constant current leads to increased losses.

To avoid additional DC/DCs the voltage level of the balance of plant (BoP) components shall be in the same range as the battery (Figure 2-6). BoP components are HV components of a FCS that are required for their operation, they include a turbocharger or air compressor and a coolant pump, beyond other components.
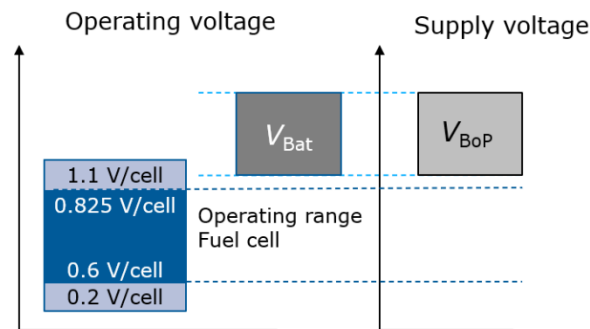
Figure 2-6: Voltage level of fuel cell, battery and balance of plant (BoP) components

The total isolation resistance is calculated by considering all isolation resistances on the HV bus which include the FCS, the battery, the turbocharger, the coolant pump, etc.

$$R_{\text{total}} = f(R_{\text{FCS}}, R_{\text{Bat}}, R_{\text{TC}}, R_{\text{CP}}, R_{\text{DCDC}}, \dots)$$

Depending on the power demand of the vehicle several FCS may be connected in parallel. A common HV architecture with two FCS is shown in Figure 2-7. Each FCS is connected via a one-directional boost DC/DC.
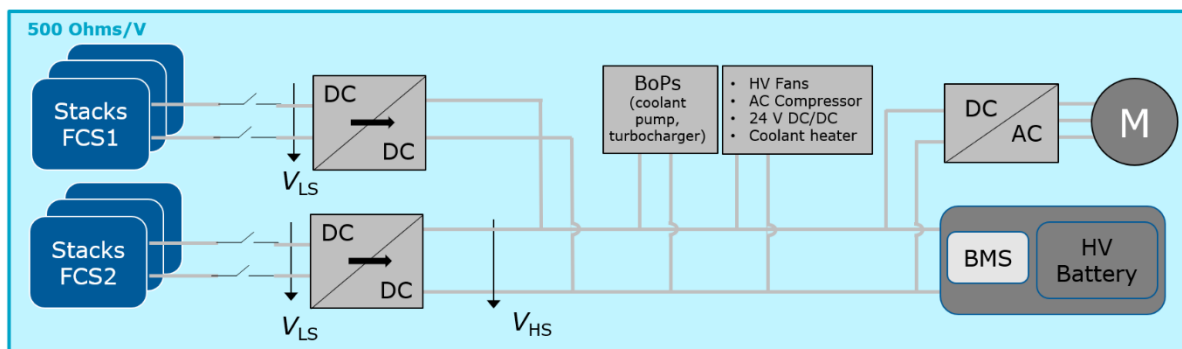
Figure 2-7: HV architecture of a FCEV with two FCS in parallel

When connecting several FCS in a system in parallel, combined isolation resistance of all FCS R_{FCS} decreases proportionally with increasing number n of FCS, see equation (2-4). That can be a challenge regarding compliance with the isolation resistance requirements towards HV safety. For combined DC and AC circuits, like that of a fuel cell system with galvanically connected DC/DC, the minimum isolation resistance is 500 Ω/Volt.

$$R_{\text{FCS total}} = \frac{R_{\text{FCS}}}{n} \qquad\qquad\qquad (2\text{-}4)$$

The option of decoupling the isolation resistance of an FCS from the rest of the HV bus by using a galvanically isolated DC/DC are discussed in chapter 5.3.

3 Fuel Cell System

A fuel cell's (FC) aim is to provide electric energy from chemical energy. In a PEMFC the chemical energy is supplied as hydrogen and oxygen. To allow operation, several additional components are required. These components and the fuel cell itself together form the so called fuel cell system, which usually has an electric interface to the outside, e.g. an HV system of an electric vehicle. This chapter's focus is an introduction to the fuel cell itself but also on the subsystems.

3.1 PEM Fuel Cell

The key information of this section is

- Basic principle and electrochemical equations
- Design and subcomponents
- Relevance for isolation resistance

The low temperature PEM fuel cell is by far the most common type in the automotive industry. It operates between 50 °C and 90 °C and is supplied with hydrogen and air. The **basic principle** is shown in Figure 3-1. The hydrogen supplied on the anode is split into hydrogen ions and electrons. The ions can move through the electrolyte while the electrons pass through the external circuit and thereby provide electric energy. Air is supplied on the cathode where the oxygen reacts with hydrogen to water (H_2O). The anode as well as the cathode reaction are facilitated by a catalyst, usually platin. The fuel cell does not only produce water as a by-product but also heat, which is related to the efficiency of the fuel cell. The theoretic possible efficiency of a PEMFC is 83 %, practical efficiencies are typically between 40 % and 60 % [14]. A 100 kW fuel cell with a 50 % efficiency will generate 50 kW heat. To remove this amount of heat an effective thermal management is essential. This is typically done with a liquid coolant flowing through the fuel cell.
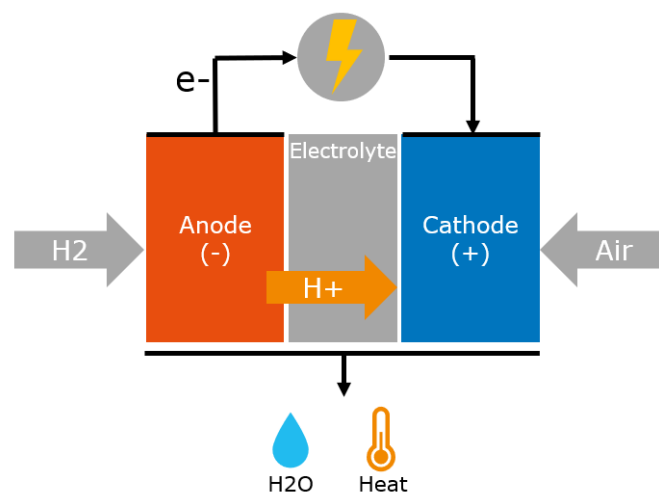
Figure 3-1: Basic principle of a PEM fuel cell

The principle can also be described by means of **electrochemical equations**. The first one, is the hydrogen oxidation reaction at the anode shown in equation (3-1). This reaction is a standard reference known as the reversible hydrogen electrode (RHE). The potential (E_{RHE}) is universally set to zero Volt [14].

$$H_2 \leftrightarrow 2H^+ + 2e^- \; E^0_{RHE} = 0 \, V \tag{3-1}$$
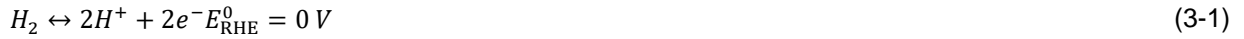
The oxygen reduction reaction (ORR) is happening at the cathode. It is shown in equation (3-2).

$$O_2 + 4H^+ + 4e^- \leftrightarrow 2H_2O \; E^0_{ORR} = 1.229 \, V \, (vs. \, RHE) \tag{3-2}$$

The highest reversible voltage for a single cell PEMFC is 1.229 V, for H_2O generated in liquid form. For gaseous water it would be 1.184 V. In a fuel cell stack both phases are present. The operating voltage is below 1 V due to various losses, which will not be discussed further within this thesis. However, more information not only on the fundamentals of PEMFCs but also on the current state of fuel cell research can be found in the book "Fuel Cells and Hydrogen Production" (2019) by Dr. Timothy E. Lipman and Adam Z. Weber [14].

In a fuel cell system, several hundred individual cells are stacked together to achieve the required power output. The cells are connected electrically in series.
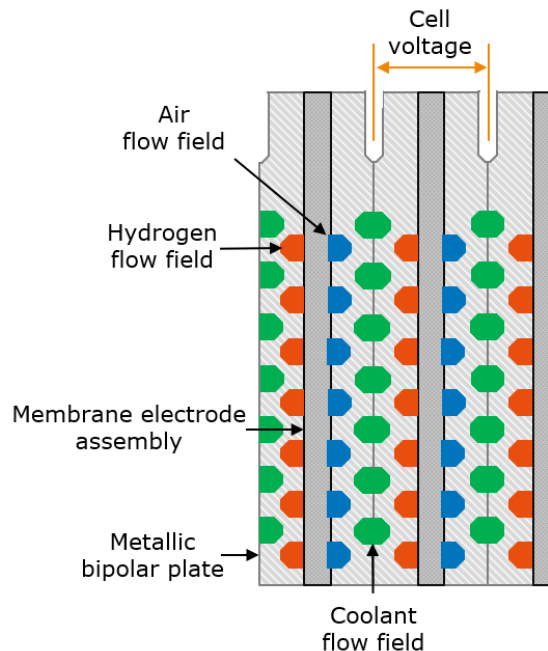
Figure 3-2: Design of a PEMFC

A single **fuel cell's main components** are the membrane electrode assembly (MEA) and the bipolar plates (BPP). The MEA is basically what is seen in Figure 3-1. It is where the electrochemical reaction takes place. The BPP separate the individual cells and connect the cell to the next one electrically. A

further task is the even distribution of hydrogen and air along the MEA, for which specific flow fields are designed.

The BPP is electrically in contact with all media paths. Therefore, all media paths are potential paths to ground, which is **relevant for the system's isolation resistance**. It is not possible to make the BPPs from a non-conductive material and therefore avoid the connection to ground. Bipolar plates are responsible for conducting electricity. In a fuel cell stack they ensure the flow of current from one cell to another. A high resistance of the plate would lead to Ωic losses, resulting in a voltage drop and thereby reducing the overall efficiency. In addition to electrical conductivity, also the thermal conductivity is key to removing the generated heat. Therefore, BPPs are either made of graphitic or coated metallic materials. [15]

3.2 Subsystems

The fuel cell requires a continuous supply of the reactants air and hydrogen to generate electric energy. Both the management of the hydrogen supply as well as the management of air supply can be summarized in subsystems. Further, the fuel cell needs a thermal management, especially to remove heat generated by the electrochemical reaction, which is the third fundamental subsystem of a fuel cell system. As the thermal subsystem is the main contributor to the isolation resistance of a fuel cell system it will be briefly described at this point and more comprehensively with its relevance for the isolation resistance in chapter 4.2
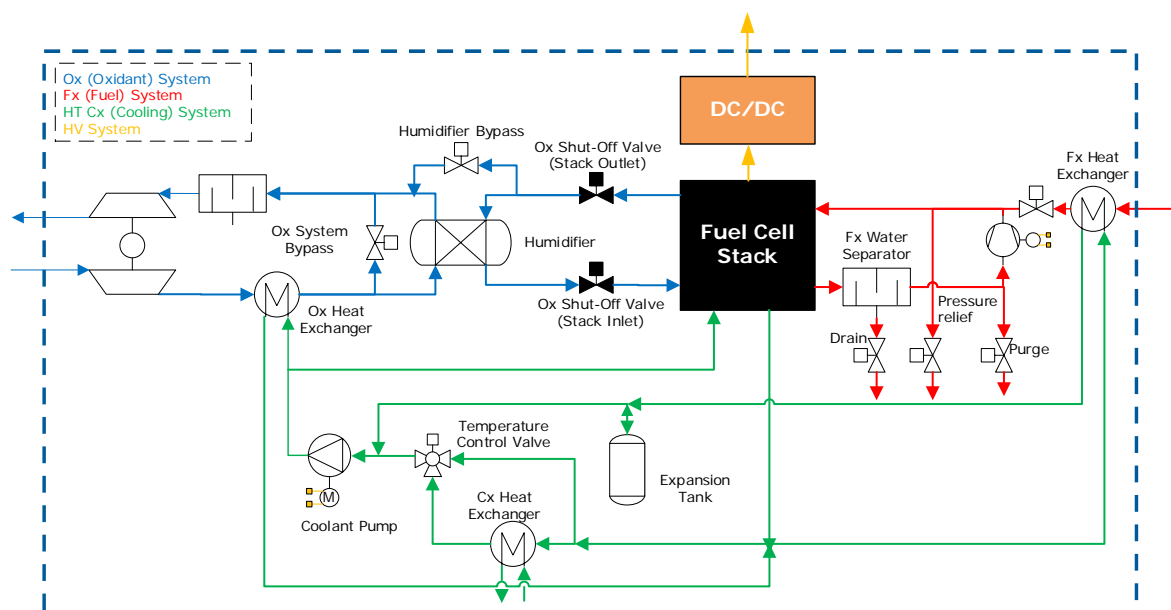
Figure 3-3: Simplified architecture of a PEM fuel cell system

The following subsystems as shown in Figure 3-3 are part of this chapter:

- Anode (hydrogen) subsystem
- Cathode (air) subsystem
- Thermal (coolant) subsystem

3.2.1 Anode (Hydrogen) Subsystem

Hydrogen enters the anode subsystem from the tank system in gaseous form. The storage itself can either be gaseous or in liquid form. The density in liquid form is higher but the storage itself is technically more complex. To increase the density of a gaseous storage, the nominal tank pressure for automotive applications is commonly at 350 bar or 700 bar [16].

The anode is pressurized to increase the partial pressure of hydrogen and enhance the reaction. The supply of hydrogen to the fuel cell is in an over stoichiometric ratio, meaning more hydrogen is supplied than is needed for the reaction. This is necessary as hydrogen depletes over time as nitrogen and water diffuses from the cathode to the anode. The difference in partial pressures drives the diffusion. Common stoichiometries are between 1.5 and 2 [17].

As the efficiency would greatly reduce if hydrogen left the system unreacted, the excess hydrogen is recirculated from the stack outlet back to the inlet. This is either done by passive or active recirculation. An active principle uses an electrically driven blower while the passive system makes use of the venturi principle including an ejector into the system. The ejector sucks hydrogen from the secondary stream due to a high velocity primary stream.

The hydrogen concentration reduces over time as hydrogen is consumed and nitrogen and water diffuse to the anode. To maintain the concentration within a desired range a purge valve is included to remove the gas mix out of the anode into the exhaust. The gas mix is replaced by pure hydrogen from the supply, thereby increasing the hydrogen concentration.

The water accumulated in the anode is partially liquid at the anode outlet. It needs to be separated to avoid liquid water entering and blocking the anode gas channels within the fuel cell. The separated water is released into the exhaust by a drain valve. Further, the hydrogen entering the anode subsystem from the supply can be heated by passing through a heat exchanger.

3.2.2 Cathode (Air) Subsystem

The air on the cathode side is also supplied in an over stoichiometric ratio. The main reason is to remove the produced water. The air is further compressed, which increases the partial pressure of oxygen at membrane. This is essential to achieve high power densities.

Generally, the humidity is an important parameter for the performance of a fuel cell. The membrane humidification determines ion conductivity of the electrolyte, which causes resistive losses if too low. Commonly, a humidifier is included in the system to allow outlet water generated by reaction to move to the inlet side.

Shut off valves at inlet and outlet of the cathode avoid air from entering the fuel cell when the system is off. This is done to increase the lifetime.

The shut off valves and further a stack bypass valves are required for state of the art starting and stopping of the fuel cell.

3.2.3 Thermal (Coolant) Subsystem

For the control of the temperature of the fuel cell a high temperature (HT) coolant loop is designed. The temperature range is between 50 °C and 85 °C [17, 18]. Additionally, a low temperature (LT) coolant loop is separately designed for cooling of electrical components like the e-machine, converters and other HV components of the FCS like the compressor in the cathode loop. Those components require lower temperatures which is why the loops are considered separately. In this thesis the HT coolant subsystem is in focus as it is in contact with HV via the fuel cell which is relevant for the isolation resistance.

The temperature control input for the fuel cell is linked to the humidity of the cathode gas stream. Gaseous water is desired but liquid water must be avoided as it can block the channels of the fuel cell. Therefore, the relative humidity shall be below 100 % or in different words the dew point of water must be lower than the gas temperature. It is not sufficient to transport excess heat away from the fuel cell. It is necessary to implement an accurate temperature control strategy for the inlet as well as outlet temperature of the fuel cell. To do so, the coolant pump and a motor driven temperature control valve, which controls the coolant flow over the radiator, are integrated in the system.

When the system is under high operational load, the ambient air undergoes significant heating due to compression. This heat is then mitigated by an appropriate heat exchanger. On the other hand, when the system is under low load, the air is warmed up to the operational temperature. Both these processes contribute to the effective humidification of the air. On the anode side, hydrogen may be cold from the tank. A heat exchanger between anode and coolant system allows heating up the supplied hydrogen. Risk of liquid water in the anode can thereby be reduced.

The coolant itself needs to fulfill several requirements, one of them being a low conductivity. To keep the conductivity low an ion-exchanger or de-ionizer is included in the system. Both the coolant and the de-ionizer are described more comprehensively in the chapter 4.2.

The characteristics of the coolant to keep in mind are the following [19]:

- Electrical conductivity
- Corrosion protection
- Thermal conductivity
- Material compatibility

3.3 Scaling of a Fuel Cell System

The electric power generated by a fuel cell can be calculated with $P = V \cdot I$ using the formulas (3-3) and (3-4) for stack current I_{stack} (3-3) and stack voltage V_{stack} respectively.

$$I_{\text{stack}} = A \cdot j$$

(3-3)

Where

A is the active area of a single cell in cm^2
j is the current density in A/cm^2

$$V_{\text{stack}} = V_{\text{cell}} \cdot n$$

(3-4)

Where

V_{cell} is the cell voltage in V
n is the number of cells

The current density j and cell voltage V_{cell} are described by the characteristics of the PEM fuel cell, they are not scalable. A typical polarization curve of a PEM fuel cell is shown in Figure 3-4. The green (●) line shows the cell voltage over the current density, the black (■) line shows the power density over the current density and the red (▲) line shows the cell efficiency over the current density. The losses lowering cell voltage and efficiency are partially activation losses, Ωic losses and mass transport losses. They increase with increasing cell voltage.

It is important to note, that the fuel cell does not provide electrical current on its own. The electric potential establishes as soon as the fuel cell is supplied. However, for current to flow it needs to be actively drawn. Mostly, the component to control the fuel cell current, and therefore power, is a DC/DC which connects the FCS to the vehicle HV bus.
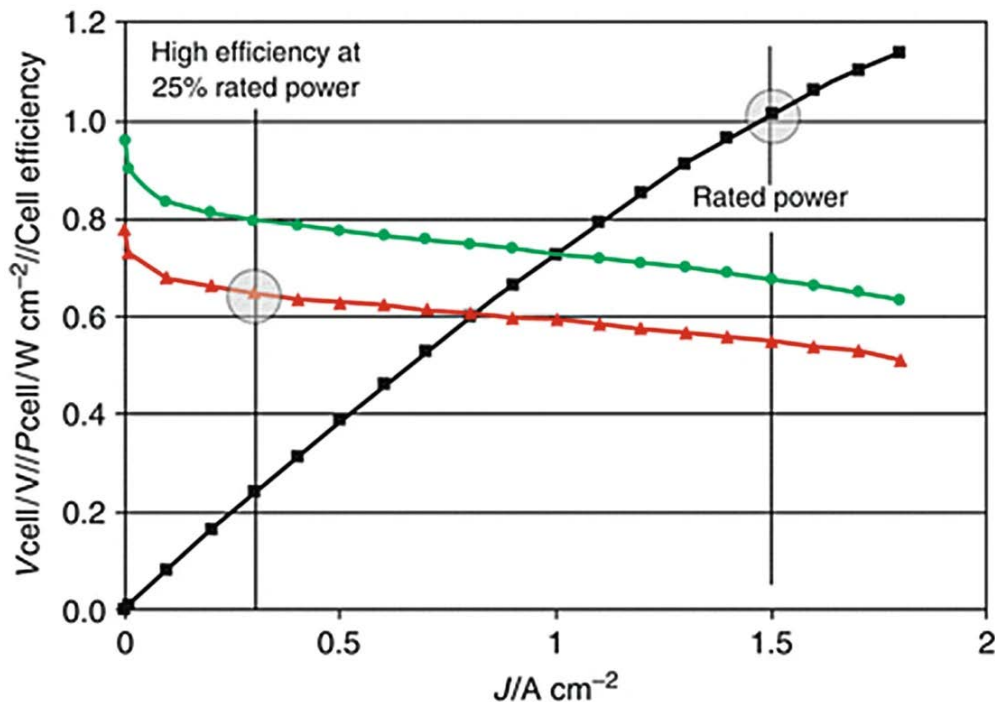
Figure 3-4: Fuel cell performance: Cell voltage (green), power density (black), and efficiency (red) versus cell current density [20]

While improvements in cell design are still made, there are physical limits to cell voltage and current density. The operating voltage, when generating current, is below 0.85 V/cell [17]. The current density at which a fuel cell operates is often at 1.5 A/cm^2 [20]. With a state-of-the-art fuel cell, operation at 2.5 A/cm^2 is also feasible [17]. However, as losses increase with increasing current density, the rated point is often chosen at a lower current density to increase efficiency. Therefore, when scaling the power of a fuel cell it is necessary to increase the active area of the cell or increase the number of cells. While active area scales the current, the number of cells scales the stack voltage. Typical automotive stacks have active areas of around 250 cm^2 [17]. With a current density of 1.5 A/cm^2 that would result in a stack current of 375 A.

Table 3-1: Limitations in scaling FCS power

Scaled parameter	Limitation
Active area → stack current	• Availability of electrical components e.g. main relays, high voltage DC/DC • Even media distribution in the cell
Number of cells → stack voltage	• Availability of electrical components e.g. main relays, high voltage DC/DC • Mechanical stability of a stack row, several cell rows can be connected electrically in series

Both scaling of current and voltage runs into limitations of available electrical components on the market. Another concern is the mechanical stability of the fuel cell stack. Commonly, up to 360 cells are stacked together [17]. However, several cell rows can be connected electrically in series when media is evenly distributed. Scaling the active area is a challenge for media distribution in the cell.

Generally, the desired stack voltage is highly linked to the HV bus voltage. As the stack operating voltage is a function of the current density, it needs to be given as a range rather than a single value.

The upper voltage limit is the open circuit voltage (OCV) at which no current is drawn. It can be up to 1.1 V/cell but is commonly around 0.9 V/cell. With an effective operating strategy, the OCV can be avoided by timing the current drawn from the fuel cell. Then, when supplying the fuel cell, the voltage builds up and stops at the idle voltage as current is drawn. The idle power is the lowest power operating point. A typical value is 0.825 V/cell. The lowest operating voltage is at the highest power point, rated power. A typical value is 0.6 V/cell. The values including typical variations are summarized in Table 3-2.

Table 3-2: Typical operating voltage ranges of a PEMFC [17, 20]

Power point	Typical voltage range
Open circuit voltage (no load)	900 to 1100 mV/cell
Idle power	825 to 875 mV/cell
Rated power	550 to 660 mV/cell

German OEMs (original equipment manufacturers) defined applicable voltage ranges in their group standards (e.g. GS 95023 by BMW, VW 80303 by Volkswagen) under which HV equipment shall work. They are based on the LV123, which was a harmonized document of test requirements for HV safety on the HV bus of all German OEMs. Today, however, the OEMs again use their group standards as the LV123 is not applicable anymore. The voltage class has a significant impact on the component design and related costs. The standardization of voltage classes leads to less variation on the market which reduces system costs. Further, the exchange of components from different suppliers is easier. The relevant ranges defined in GS 95023, chosen exemplarily, are shown in Table 3-3, the full table is shown in the appendix in Table 2. Currently, the group standards have the highest voltage class of HV_3 with an upper voltage of 750 V. The ISO 21498-1 [21], which is valid internationally, has adopted the LV123, but defined more and slightly different voltage ranges as shown in Table 3-4. The highest voltage class is B_1250, with an upper operating voltage at 1250 V. Currently, BoP HV components required for fuel cell systems, like coolant pump and compressor, are available mostly for HV_2b and HV_3 voltage range. HV components are usually electrically connected on the HV bus which would then either require the same voltage range of the battery and propulsion or an additional DC/DC to connect the components, which adds complexity.

Table 3-3: HV voltage ranges according to GS 95023 [22]

HV voltage ranges	Unit	HV_1	HV_2a	HV_2b	HV_3
Maximum operating voltage	V DC	200	360	470	770
Upper restricted operational capability	V DC	191 to 200	341 to 360	451 to 470	751 to 770
Unrestricted operational capability	V DC	90 to 190	170 to 340	250 to 450	520 to 750
Lower restricted operational capability	V DC	80 to 89	160 to 169	200 to 249	450 to 519

Table 3-4 further shows which semiconductors fit to the relevant voltage range. It again highlights the limitation of scaling the size of the fuel cell by adding cells, as it must fit to other technologies of components that are available on the market [21].

Table 3-4: HV voltage ranges according to ISO 21498-1 and related semiconductor technologies [21]

Voltage sub-class	Upper voltage limit (RESS or electric propulsion system)	Related semiconductor technology — Example
B_220	U ≤ 220 V DC	MOSFETs 300 V breakdown voltage
B_420	U ≤ 420 V DC	Standard IGBTs and MOSFETs 600 V breakdown voltage
B_470	U ≤ 470 V DC	Selected IGBTs 700 V breakdown voltage and dedicated module technology
B_750	U ≤ 750 V DC	IGBTs 1 200 V breakdown voltage
B_850	U ≤ 850 V DC	IGBTs 1 200 V breakdown voltage
B_1250	U ≤ 1 250 V DC	IGBTs 1 700 V breakdown voltage

Exemplarily, the number of cells for a HV3 architecture and a boost DC/DC between FC and HV bus is calculated in Figure 3-5. The minimum voltage is mostly defined by the battery. Then, for a boost architecture there is a minimum voltage difference between HV bus and FCS, in this case 20 V. With the definition of the idle power point the number of cells can be calculated using equation (3-4). The number of cells for a HV3 architecture is 606 cells. The cells number can be split into two rows to achieve mechanical stability.
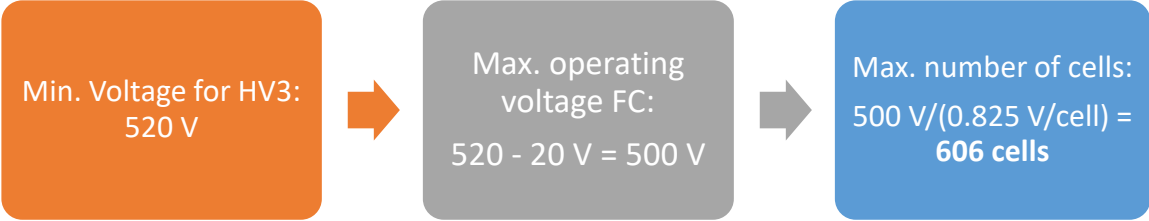
Figure 3-5: Exemplary derivation of cell number

4 Isolation Resistance of a Fuel Cell System

In a fuel cell system reaching the legal requirements for the isolation resistance is especially challenging. All media paths (air, fuel/hydrogen, coolant) are in contact with HV. The main contribution for low isolation resistances is the electrical contact between the HV of the fuel cell and the coolant sub system. However, also the anode and the cathode can be causes for low isolation resistance, which is a part of this chapter. With regards to the coolant sub system, the contributors to the resulting isolation resistance are discussed.

4.1 Anode and Cathode Condensate

The product water of a fuel cell is produced at the cathode. However, due to diffusion mechanisms the water partly moves to the anode. As the fuel cell is operated at around 80 °C the water is mostly present in gaseous form. Depending on operating conditions e.g. during warm up where temperatures do not yet meet the set value, liquid water is to be expected. The product water from the electrochemical reaction from hydrogen and oxygen is ultra-pure, no ions are involved. That theoretically leads to an electrically non-conductive liquid or gas.

Anyways, in some cases a condensate path to a grounded point near the anode or cathode outlet can lead to an isolation fault. That grounded point could be metal piping or a sensor which has a ground connection over the control unit. If this is the case, the condensate became conductive.

Conductive product water is a result of degradation mechanisms within the fuel cell. The most commonly used materials are perfluorosulfonic acid (PFSA) membranes such as Nafion® (DupontTM), GoreSelect® (GoreTM), Aciplex® and Flemion® (AsahiTM). [23]. Additives from the membrane can leach into the product water during operation from thermal decomposition. But not only degradation can lead to contamination of product water, also new stacks can show initial leaching from coatings. Acidic side chains increase the electrical conductivity of the product water [24].

4.2 Coolant System

In this chapter the relevance of the coolant loop for the system's isolation resistance is evaluated. The isolation resistance of a coolant-filled pipe is a measure of the electrical conductivity σ of the coolant, the cross section A_i of the pipe and the length l_i of the pipe.

$$R_i = \frac{1}{\sigma} \cdot \frac{l_i}{A_i} \tag{4-1}$$

As there is a regular electric contact between coolant and HV, grounded components in the coolant loop represent a path to ground. The resistance can be calculated with a network of elements, each

calculated using formula (4-1). The network evaluation uses basic rules for serial and parallel connection of resistances as shown in Table 4-1: Serial and parallel connection of resistances.

Table 4-1: Serial and parallel connection of resistances

Serial connection	Parallel connection
$R = R_1 + R_2 + \cdots + R_n$ (4-2)	$\dfrac{1}{R} = \dfrac{1}{R_1} + \dfrac{1}{R_2} + \cdots + \dfrac{1}{R_n}$ (4-3)
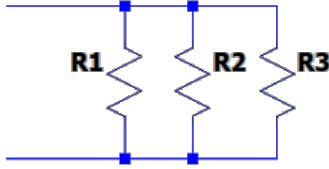
The following sub chapters shall give an overview of the influences on the isolation resistance based on formula (4-1):

- The coolant pipe length, determined by the position of the grounding points,
- The conductivity of the coolant, and
- The cross section of the coolant pipe.

4.2.1 Grounding Points

For the calculation of the length, the starting point is the stack inlet as well as the stack outlet. The end points are the grounded points of the components in the coolant loop. The coolant hose material is non-conductive.

Generally, it's the first grounded point that is relevant. But as there are two starting points (stack inlet and stack outlet), there are also at least two relevant first grounded points. If the first grounded point is after a junction, there may be even more than two relevant first grounded points, as there are resistances in parallel. If there are two grounded points in series, only the first one is relevant for the calculation.

Potential grounding points of the coolant sub system according to Figure 4-1 are:

- Sensors, connected to ground via the control unit
- Coolant pump, conductive housing of HV components are connected to ground via equipotential bonding according to ISO 6469-3 [7]
- Temperature control valve, connected to ground via equipotential bonding if there is a conductive connection to the coolant
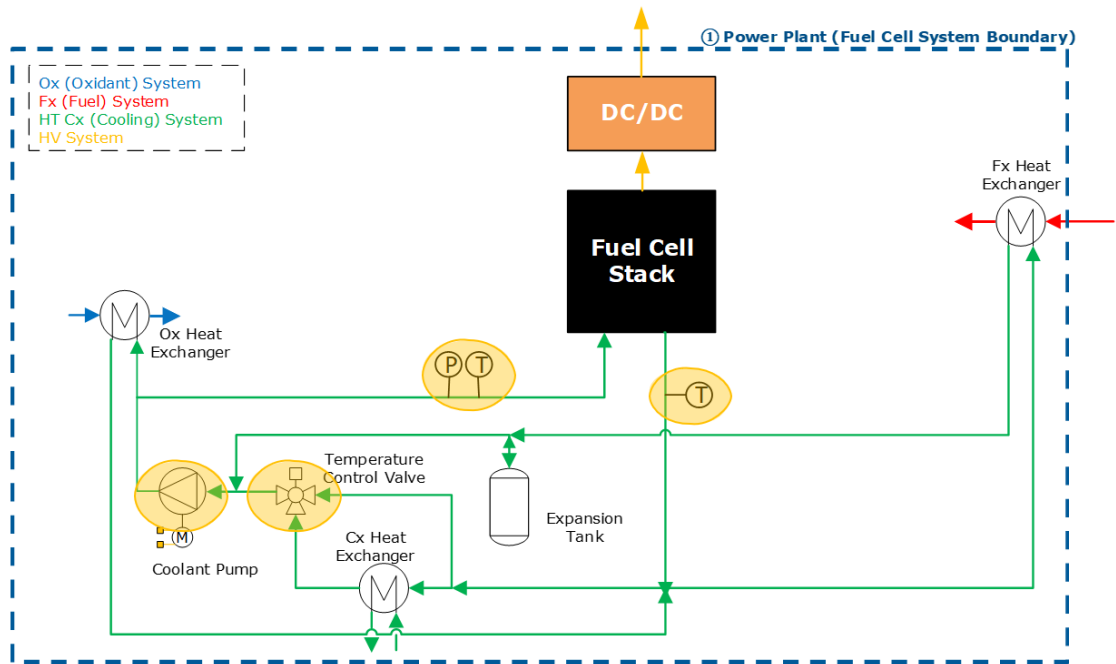
Figure 4-1: Potential grounding points in the coolant loop, marked in yellow

Further, conductive joints or connectors must be grounded if they are in contact with the coolant.

4.2.2   Coolant Conductivity

The second influence on the isolation resistance in the coolant path is the electrical conductivity of the coolant. The electrical conductivity is a measure of the ionic concentration [25]. The conductivity of a fuel cell coolant is in the range of 0.1 µS/cm to 50 µS/cm. Depending on the application and the isolation resistance targets, the conductivity targets may be < 5 µS/cm or even < 1 µS/cm [26]. The influences on the coolant conductivity are diverse. They are

1.   Materials in contact with coolant
2.   Deionizer (resin) in the coolant loop
3.   Composition of the coolant
4.   Temperature of the coolant
5.   Cleanliness of components
6.   Degradation of the fuel cell system

4.2.2.1   Materials in Contact with Coolant

Ion leaching from metal or nonmetal components with which the coolant is in contact with will increase the electrical conductivity. Therefore, the requirements for materials used in the coolant loop which are also in contact with coolant are important. The materials shall have a low extraction level of inorganic as well as organic species. This can be verified by a hot water extraction test. Further, the materials must be resistant to deionized water with moderate acidity with pH values from 5 to 7.

Prominent materials used in fuel cell coolant systems include

- Stainless steel 316L, 304L
- 6061 aluminum
- EPDM
- PTFE
- PPS
- PP

This list provides a few examples for metals, thermoplasts and elastomers. It is not exhaustive. Sometimes the evaluation whether a material is suitable also depends on the contact area with the coolant. All materials must be evaluated: components, hoses, connectors, sealings, lubricants, etc.

The coolant hose material has a special importance when it comes to conductivity as the surface in contact is the largest. Coolant hoses can be either wrapped or extruded. Wrapped hoses are made of several layers. The important one for the conductivity is the inner layer. Common materials for coolant hoses are:

- Platinum cured silicone (inner layer for wrapped hoses)
- FKM (wrapped hoses)
- EPDM (extruded hoses)

4.2.2.2   Deionizer (Resin) in the Coolant Loop

The ion exchange resin is used to remove ionic substances from the coolant. Fuel cell systems commonly use mixed bed resins which exchange anions as well as cations. Thereby, the conductivity is kept low. There are two factors to consider for deionizers. First, the capacity to exchange ions is limited, which means it is still essential to minimize the ingress of ions. Second, not all ions can be exchanged by the deionizer. Therefore, a rest conductivity will always remain. The level of it can differ from system to system. [27]

One way to assess the capacity of the deionizer is to analyze the amount of ions in a fuel cell system by taking a coolant sample. The amount of ions after running the system for defined number of hours/days compared to the ion exchange capacity allows an estimation of the deionizer lifetime. This is a very rough estimate as the ingress of ions will not be constant over time. The initial commissioning period should not be taken as a reference as the concentration of ions may be higher initially. If time allows, the lifetime of the deionizer can also be assessed by running the system until the conductivity increases, which will then be the approximate runtime for future systems.

4.2.2.3   Composition of Coolant

A fuel cell coolant is a mix of ethylene glycol and deionized (DI) water mainly. Those two components typically make up for around 97 % of overall volume [19].

The percentage of each is equal (50/50) for freezing points around -40 °C. Depending on the required freezing point the portions can vary. For higher freezing points, less glycol is required. Glycol therefore is considered as an antifreeze additive. If a freezing point of 0 °C is acceptable, deionized water solely

can be used as a coolant for fuel cells. This is often done at the test bed or in stationary systems where the ambient conditions are stable. [19, 28]

The remaining 3 % are additives. Those ingredients are the primary differentiating factor for coolants of different manufacturers. The functions include corrosion protection and pH buffering. [19]
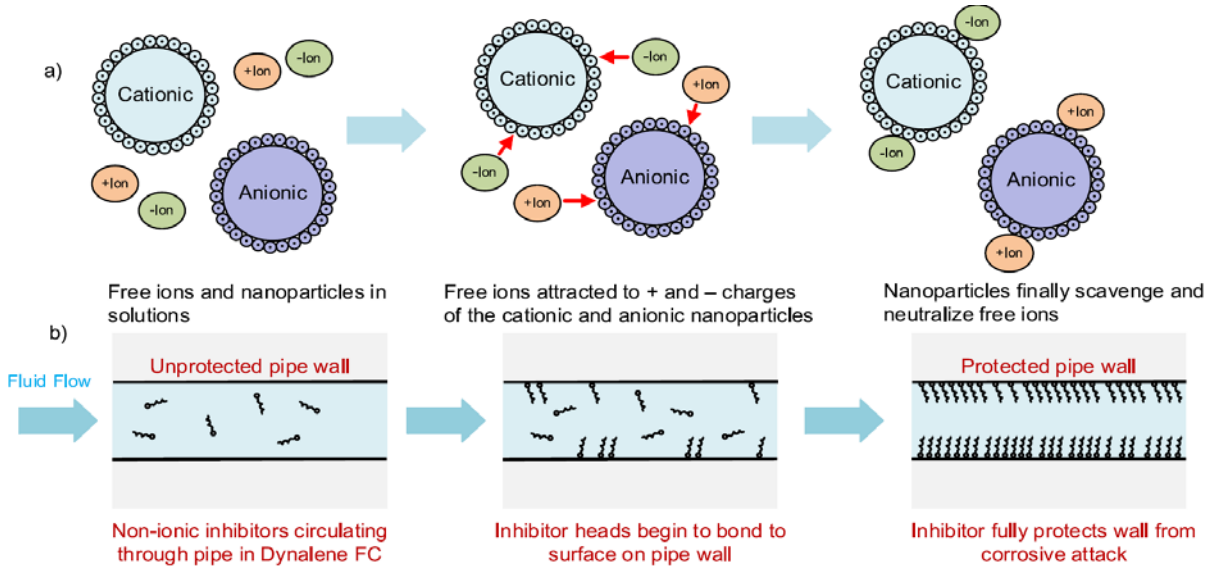
Figure 4-2: Mechanisms to lower the electrical conductivity using; (a) Nanoparticles; (b) Inhibitors [28]

While a low electrical conductivity of the coolant is a major advantage for the isolation resistance, the corrosion inhibition needs to be secured as well. Figure 4-2 shows two possibilities to lower the electrical conductivity. First possibility is by nanoparticles as additives in the coolant. Highly charged ionic nanoparticles are added to the coolant and attach to free ions. Thereby, they are neutralized which lowers the electrical conductivity. The second way is using non-ionic inhibitors which attach to the surface of components and piping and thereby act as protection against corrosion.

When using a coolant with ionic nanoparticle additives a deionizer is not required [28]. This, however, is not common in systems designed today. The main reason is the elevated base electrical conductivity of the coolant as it's loaded with ions. The level of electrical conductivity is > 10 µS/cm [29] which is considered already quite high for fuel cell systems.

4.2.2.4   Temperature of the Coolant

Generally, the relationship between the coolant temperature and the electrical conductivity of the coolant is exponential. However, in the range between 20 °C and 80 °C, at which a PEMFC mainly operates the relationship is linear. The increase of conductivity per degree Celsius is approximately 0.5 µS/cm per degree Celsius for the example in Figure 4-3.
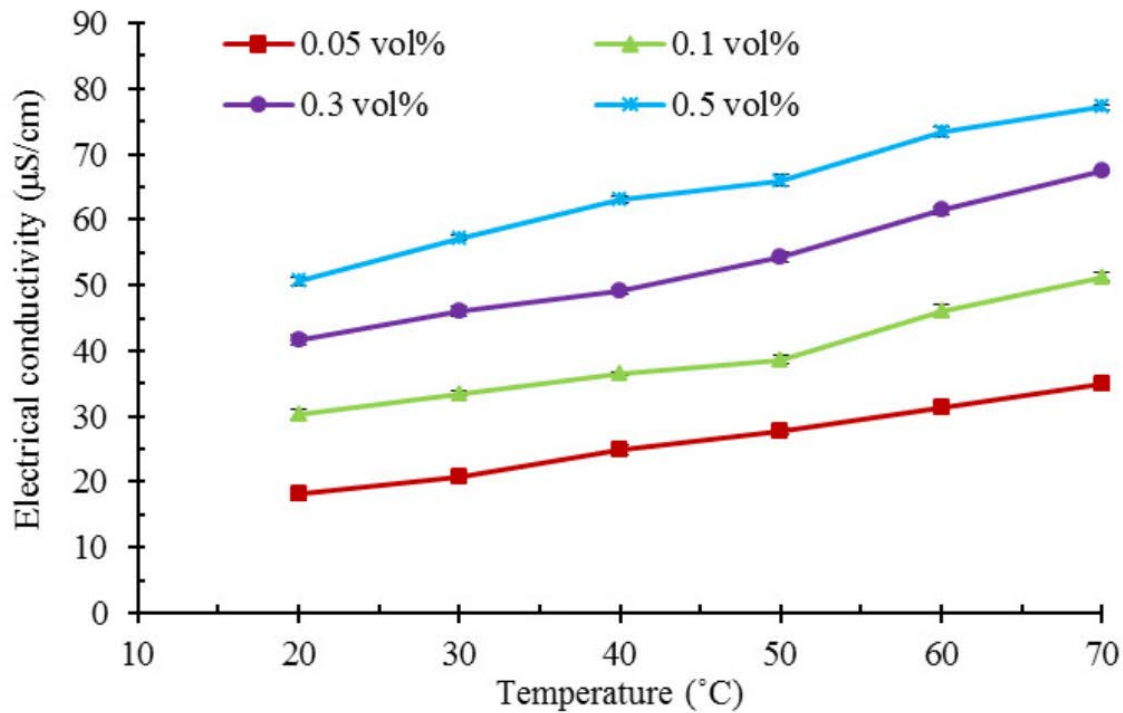
Figure 4-3: Relationship between electrical conductivity and temperature of a 50/50 mix of ethylene glycol and DI water and different loading of nanoparticles [30]

One common fuel cell coolant is the *Freecor EV Micro* 10 from Arteco. It shows an electrical conductivity of 0.5 µS/cm at 25 °C and 2.2 µS/cm at 80 °C according to ASTM D1125, which is a standard test method for assessing the electrical conductivity and resistivity of water [31]. For the Arteco coolant the increase in conductivity per degree Celsius is only 0.031 µS/cm.

4.2.2.5 Cleanliness of Components

Newly build components or even already used components typically contain residual amounts of metal contaminants, machine oil, lubricants, flux, solder, dirt, or other particulates. It is important to remove such particles and films before assembly of the fuel cell system's coolant loop. Unremoved contaminants may lead to degradation of the coolant or of other components, especially of the fuel cell stack [32].

Cleaning of the components can be done by putting them in an ultrasonic bath filled with DI-water, preferably at high temperature as contaminants are easier to remove. Further, components can be cleaned on a flow testbed. Again, preferably at high temperature and with DI-water. As a quick solution, single components can be cleaned with isopropanol, for example if only one component is exchanged. Cleaning can also be done at the supplier's place. Then, the cleanliness has to be specified and the packaging has to protect against re-contamination. If the system is already assembled, flushing the system with DI water is also possible. In this case it is important to limit the residual water in the system after flushing as it will change the coolant's properties. The freezing point could be higher than intended.

4.2.2.6   Degradation of the Fuel Cell System

Components in the coolant loop, the fuel cell stack and the coolant itself age with time. Collected contaminants on the bipolar plates or ions produced by the oxidation of glycol increase the electric conductivity of the coolant [28]. The electrical conductivity will also increase if the deionizer capacity is exhausted.

4.2.3   Cross Section of Piping

The cross section is a relevant parameter for the calculation of the isolation resistance as described in equation (4-1). The formula for the cross section $A = \pi \cdot r^2$ highlights the importance of the inner radius r of the piping.

The definition of the piping diameter is mainly influenced by the flow and pressure drop requirements of the coolant loop. Therefore, there the diameters cannot be chosen based on isolation resistance requirements. However, during component selection standard sizes with the next bigger diameter are often chosen which leads to bigger diameters than required. An awareness for the topic is essential to avoid unnecessary reduction of the isolation resistance. In many cases when choosing between two available diameters, the next smaller one may also be sufficient.
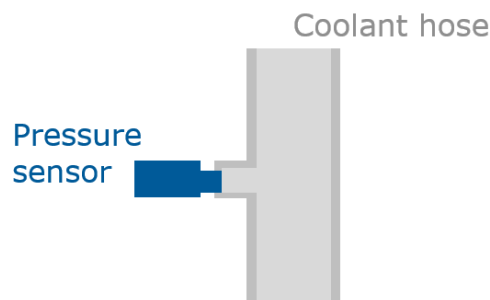
Figure 4-4: Small diameter split for pressure sensor

Another way to use the influence of the cross section is to put sensors into the smaller piping if possible. For pressure measurements the position of the sensor can be chosen more freely within a section of the same pressure. In case a section includes a junction, it is recommended to put the sensor into the pipe with the higher resistance. Thereby, the length as well as the cross section are relevant. If necessary, it is also possible to put a pressure sensor in a dedicated sense line pipe with a small diameter which sole purpose is to increase the resistance to the grounded sensor.

For temperature measurements the position influences the result and shall be chosen according to the interest.

5 Measures to Improve the Isolation Resistance

In this chapter, the possibilities to improve the isolation resistance of a fuel cell system will be assessed. The focus in this chapter is on possible solutions while in the previous chapter the general influences are discussed. The measures discussed in this chapter are:

- Isolation of components from ground
- Reduction of coolant conductivity
- Galvanic isolation on the HV bus
- Implementation of virtual sensors to replace physical sensors

5.1 Isolation of Components From Ground

The benefit of isolating components from ground and the type of components commonly grounded in the coolant loop is discussed in chapter 4.2.1. In this chapter solutions for not having to ground components are discussed.

The negative pole of the low voltage is usually connected to ground. If there is a conductive connection between coolant and the component, it has a connection to ground. It can be:

- Coolant pump with conductive rotor blades or housing
- Sensor with conductive sensor tip
- Temperature control valve with conductive disk or housing

Exemplarily, ways to isolate a sensor from ground are given in Figure 5-1. As the coolant is considered as an HV component, the sensor shall meet the requirements related to

- Electrical insulation,
- Clearance,
- Creepage distance,
- Rated impulse withstand voltage, and
- Parasitic energy storage

for the relevant voltage class.
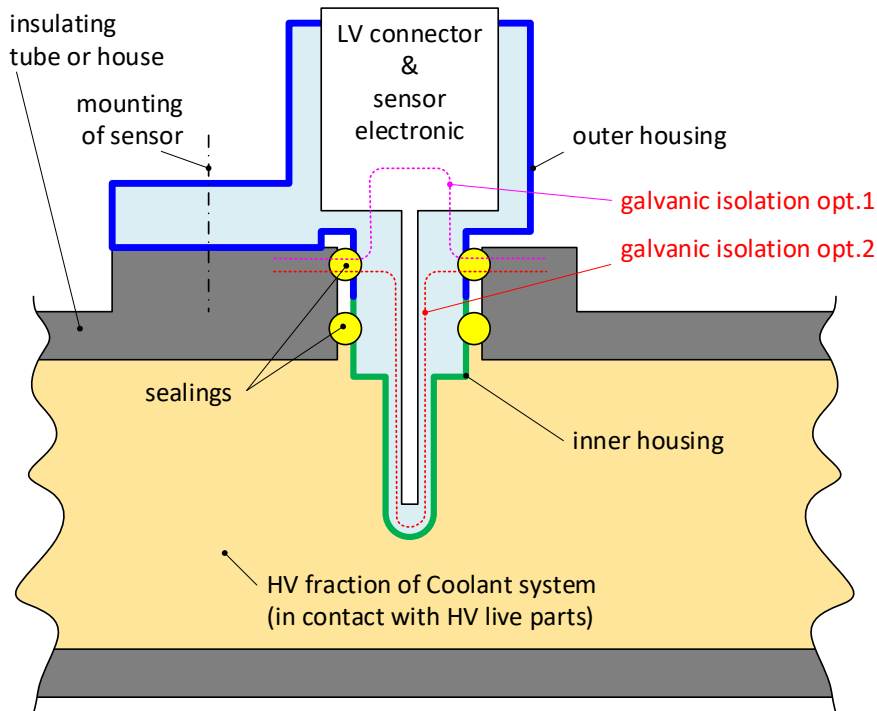
Figure 5-1: Galvanic isolation of a sensor in the coolant loop

The requirements above shall be fulfilled between the inner housing surface (green) of the housing and

- all LV connector pins (and LV sensor electronic if applicable),
- conductive connector housing (if applicable),
- all conductive elements of outer housing of the sensor (if applicable).

The options to implement the galvanic isolation are 1) by implementation in the sensor electronics or 2) by avoiding conductive contact with the medium. The second option is not always feasible as the functionality can be influenced by changing the material of the sensor tip. A temperature sensor tip can be encapsulated in a polymer housing, however, as the thermal conductivity of the material is low also the response will be slow.

5.2 Reduction of Coolant Conductivity

The influencing parameters for the coolant conductivity are described in chapter 4.2.2. One can distinguish between basic and complex choices for low coolant electrical conductivity.

The basic choices include cleaning of components before assembly and the use of materials with low ion concentrations leaching. Both are described within chapter 4.2.2. with examples for suitable materials and cleaning procedures.

The complex choices refer to the interactions between materials, the coolant and the deionizer resin (Figure 5-2). When targeting conductivities below 2 µS/cm it is essential to investigate the interactions between the choices being made. To do so, testing on a sub scale level is helpful.
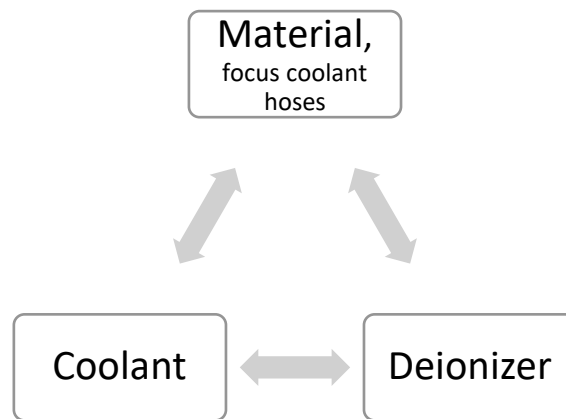
Figure 5-2: Interactions between material, coolant and deionizer resin

The interactions between the material, coolant and deionizer resin are of special importance. The deionizer and the coolant interact as the ions out of the coolant are exchanged in the deionizer. Depending on the resin used, interactions may cause the additives from the coolant to be exchanged too. The materials used influences the deionizer indirectly by the ions being dissolved in the coolant. However, the type of ions should be suitable for the deionizer to avoid higher levels of conductivity.

Generally, when conductivities below 2 µS/cm are required to achieve requirements for isolation resistance for HV safety a more generation approach for the fuel cell system design is highly recommended. That allows for optimizations when learning about the complex interactions.

5.3 Galvanic Isolation on the HV Bus

The FCS is mostly connected to the HV bus via a DC/DC. An introduction is given in chapter 2.4. This chapter focuses on the DC/DC and its effects if it is galvanically isolated. The DC/DC is specified by various characteristics:

- **Buck, buck-boost or boost**: describes the ratio from input voltage to output voltage. For higher output than input it is a boost DC/DC, for lower output than input it is a buck DC/DC. If both is possible the correct description is buck-boost. Buck-boost architectures require a second set of power modules which is why it shall be avoided if possible.
- **Uni-directional or bi-directional:** describes the direction of the energy flow. If both directions are possible, it is a bi-directional DC/DC. For FCS uni-directional DC/DCs are sufficient.
- **Galvanically connected or isolated:** The standard type is a galvanically connected DC/DC. In that case the input and output of the negative line of the DC/DC is connected through. For galvanically isolated DC/DC the input and the output are separated.

The separation of input and output leads to a separation of ground potentials. The advantage is that the isolation resistance of the FCS can be considered as a closed system. The isolation resistance of the HV bus is another closed system to consider. The consequences on the requirements are shown in Figure 5-3.
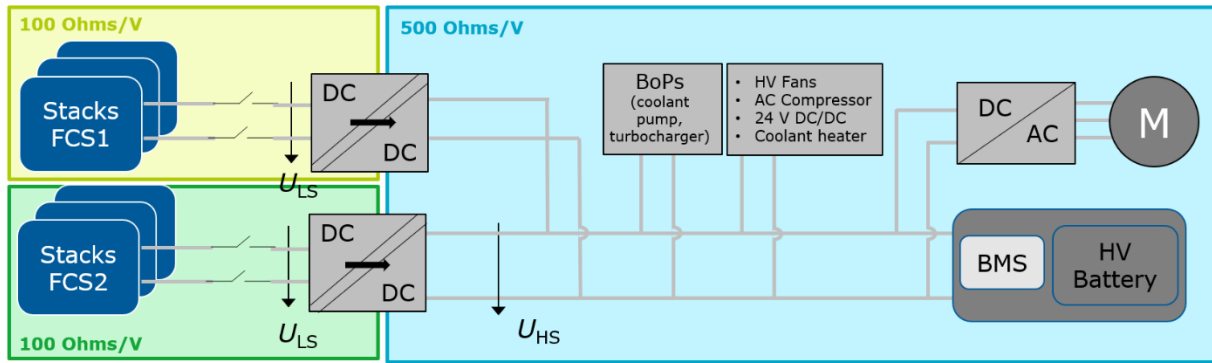
Figure 5-3: Isolation resistance requirements after ISO 6469-3 [7] for galvanically isolated FCS

When only looking at the isolation resistance it is clearly advantageous to use an isolated component. However, there are several drawbacks to consider.

Brievly, they are size, weight, cost and efficiency. Figure 5-4 aims to explain the rationale. The galvanic isolation barrier requires a conversion of DC/AC and back from AC/DC. Therefore, additional components are required. The overall efficiency reduces with each conversion step: the power oscillation, the transformation and the rectification. In most cases, the efficiency of a galvanically isolated DC/DC will therefore be lower than a galvanically connected one. Consequently, the choice of a galvanic isolation of the fuel cell must be considered carefully.

$$\eta = \frac{P_{OUT}}{P_{DD}} = \eta_{OSC} \cdot \eta_{TRASF} \cdot \eta_{RECT}$$
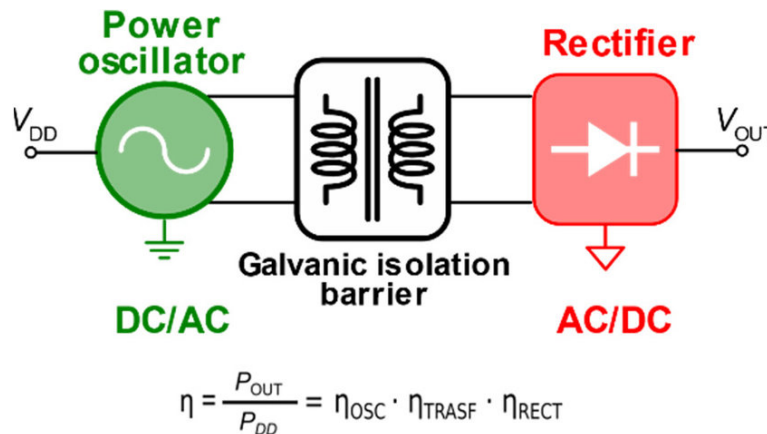
Figure 5-4: High level schematic of a galvanically isolated DC/DC [33]

5.4 Implementation of Virtual Sensors

The sensors in the coolant loop include pressure and temperature sensors. For the following potential grounded points in the coolant loop of a fuel cell system, virtual sensors are used for AVL's fuel cell system controls:

- Temperature sensor at the stack outlet
- Temperature sensor at the stack inlet

For the pressure sensor at the stack inlet currently no virtual sensor is available. In the following sub chapters the virtual sensors for the temperature at the stack inlet and outlet are discussed.

5.4.1 Temperature Sensor at the Stack Outlet

The coolant temperature at the stack outlet shows very good correlation with the air (cathode) temperature at the stack outlet. Exemplary measurement data from AVL research projects is shown in Figure 5-5. The orange line indicates zero deviation. During warmup, between 50 °C and 60 °C there is a negative offset. The shade of the blue indicates the stack current. Not visible in the plot but still relevant is the fact that the air temperature sensor shows better dynamic response. Therefore, even if there is an offset, the coolant sensor is not necessarily always the better one.
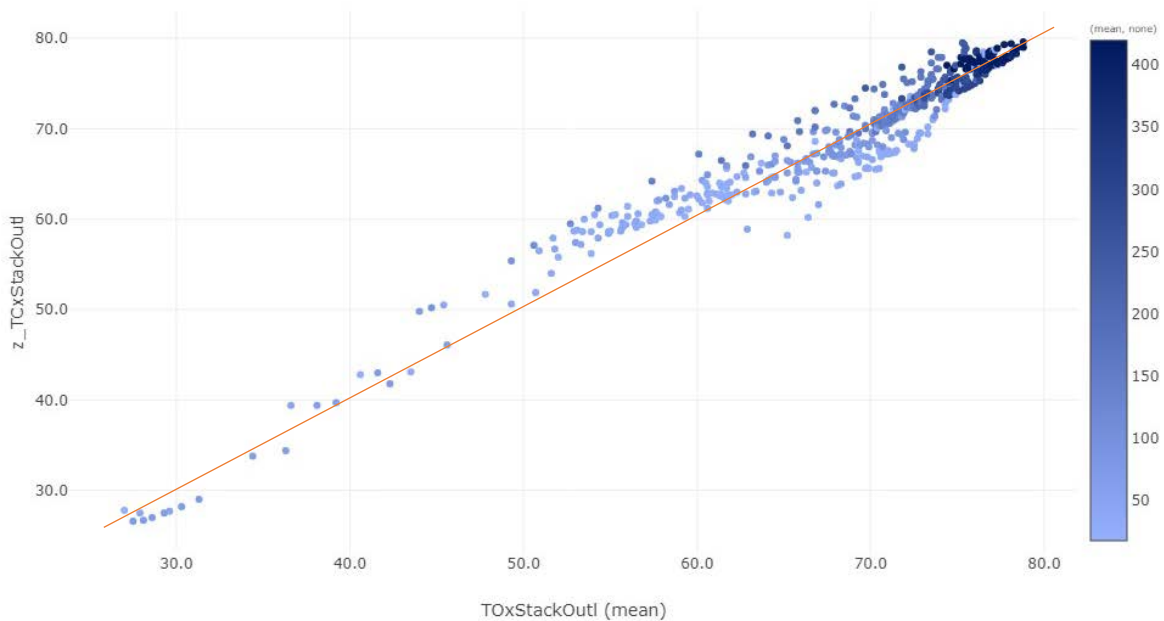
Figure 5-5: Coolant temperature (z_TCxStackOutl) over air temperature (TOxStackOutl) at the stack outlet (AVL measurement data)

5.4.2 Temperature Sensor at the Stack Inlet

The temperature sensor at the stack inlet can be modelled using the temperature sensor at the radiator outlet as well as the position of the temperature control valve. As the media (coolant) and therefore its properties are the same, the output temperature from two inlet streams follows basic mixing rules.

$$T_{out} = \frac{T_1 \cdot Q_1 + T_2 \cdot Q_2}{Q_1 + Q_2} \qquad (5\text{-}1)$$

The volume flow Q can be exchanged by the position of the temperature control valve. The position of the temperature control valve is proportional to the flow. If there is a non-linearity, an additional correction via a map is required. In principle, the model can be described as shown in Figure 5-6. Instead of the coolant (Cx) outlet temperature the air (Ox) outlet temperature can be taken as described in the previous chapter 5.4.1.

There may be corrections necessary if there are air or hydrogen heat exchangers in the loop, like shown in Figure 3-3.

$$T_{\text{Cx Outlet}} = T_{\text{Ox Outlet}}$$

$$T_{\text{Rad Outlet}} \qquad T_{\text{Cx Inlet}}$$

$$\boxed{Pos} \quad 0 < \text{Pos} < 1$$
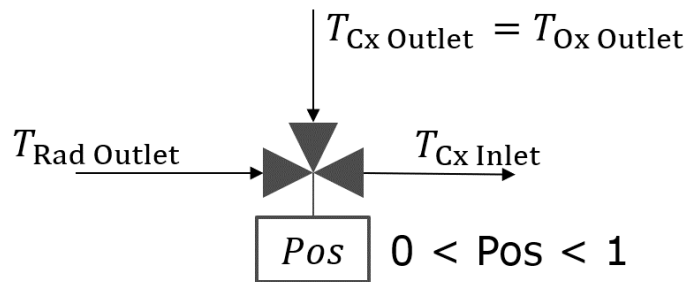
$$T_{\text{Cx Inlet}} = T_{\text{Rad Outlet}} \cdot Pos + (1 - Pos) \cdot T_{\text{Cx Outlet}}$$

Figure 5-6: Model for a virtual coolant stack inlet temperature sensor

The measurement results for the virtual coolant stack inlet temperature sensor are shown in Figure 5-7. The green and black dots show different test runs, both from stationary load changes (IV-curves). At 59 °C the system is in a stop mode, which leads to a cool down of the air path compared to the coolant path. No negative effect on operation is noticed from the resulting offset.
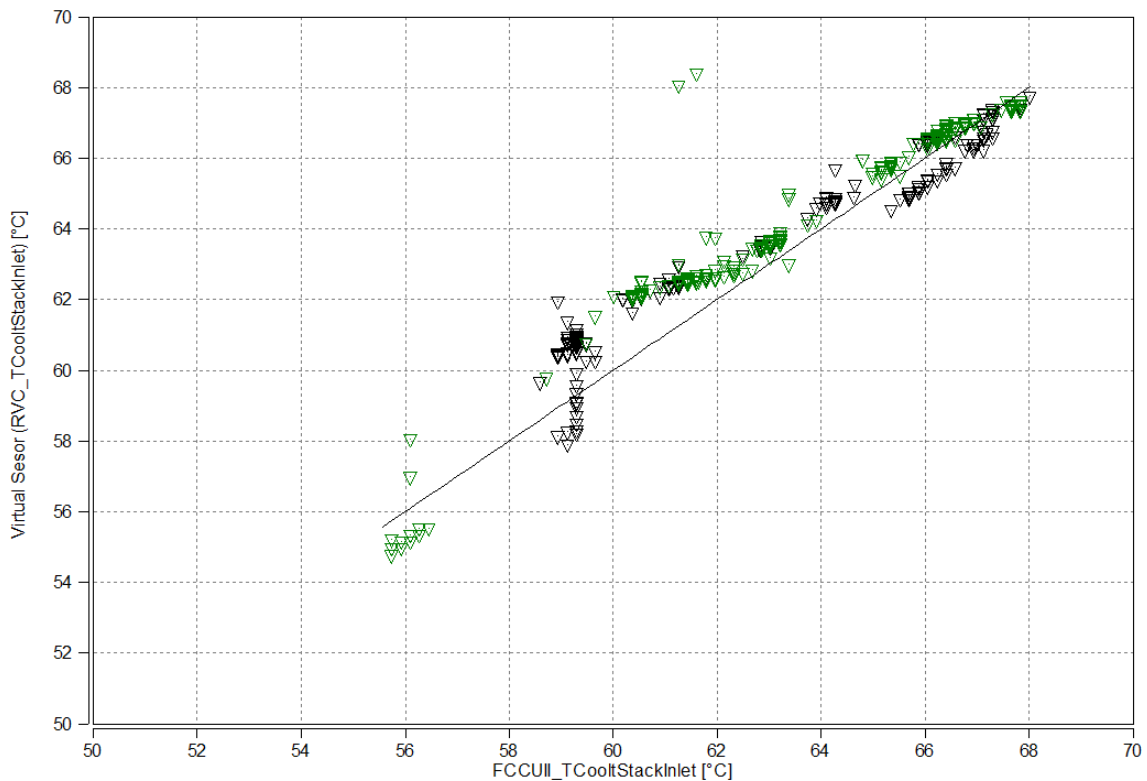
Figure 5-7: Virtual coolant stack inlet temperature over the measured coolant stack inlet temperature (FCCUII_TCooltStackInlet)

The quantitative effect on the isolation resistance of the four measures introduced in this chapter has to be evaluated project-specifically as the initial conditions vary. One such evaluation is done within the case study of the AVL Fuel Cell Demo Truck described in chapter 7.

6 Isolation Resistance Calculator

In this chapter a model of the isolation resistance of a PEM fuel cell system for the estimation of the system's isolation resistance, especially in an early design stage, is introduced. The model is set up in Microsoft Excel with the basic element being a network of serial and parallel resistance segments modeling the coolant path of the fuel cell system. To assess whether the intended design fulfills the isolation resistance requirements, an isolation resistance model is an essential element. Furthermore, the isolation resistance calculator can be used to assess the effect of specific measures, like removing a sensor, on the isolation resistance. An additional element of the calculator is the analysis of the isolation resistance and conductivity. The goal is to keep it as simple as possible for usability and to allow quick judgements in an early development phase.

The isolation resistance calculator consists of two elements, which are also two spread sheets in excel:

1. **The isolation resistance model**, which intention is to set up the resistance network and grounding points. It should allow evaluation of the change in isolation resistance when adapting the existing grounded points. The isolation resistance is calculated for a chosen reference conductivity.
2. **The isolation resistance and conductivity analysis**, which intention is to allow judgment whether the legal requirements are fulfilled with the established model and if not, what the maximum conductivity would be to comply.

Both elements are introduced with the following sub chapters for each of them:

- Inputs and outputs,
- Layout, and
- Features.

6.1 Isolation Resistance Model

The research question "How can the isolation resistance of a PEM fuel cell system be modelled?" is addressed in this chapter. A model using a resistance network is used as it allows modeling the isolation resistance based on (preliminary) 3D-layouts which fits well into the development process of a PEMFC system.

6.1.1 Inputs and Outputs

As shown in Figure 6-1, the inputs into the model are the coolant conductivity (for which the calculation shall be done), the 3D data separated in segments and the defined grounded points. Each segment from the 3D data has a specified cross section and length. Together with the coolant conductivity a resistance for each segment is calculated. With the information of the precursors and grounded points the resistance network can be calculated. The output is the total isolation resistance of the coolant loop.
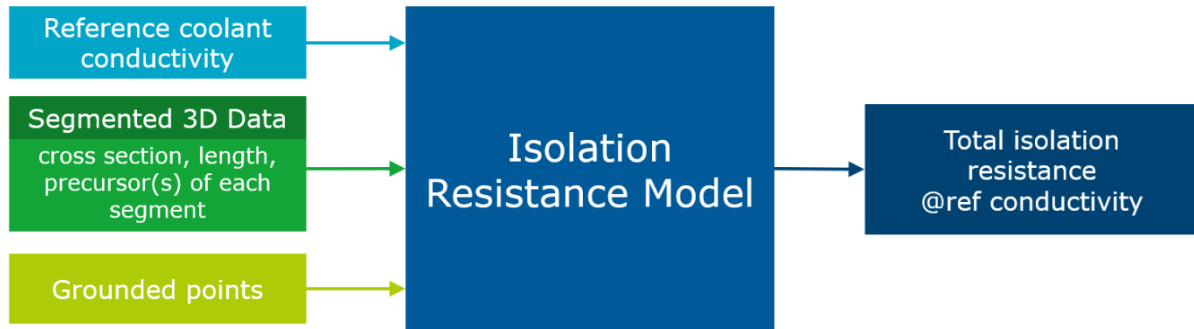
Figure 6-1: Inputs and outputs of the isolation resistance model

6.1.2 Layout

The layout for the isolation resistance model is shown in Figure 6-2. For the set up exemplary data was used, however, the data chosen is close to real data.

The yellow background colored cells are input fields, the green background colored cells are output fields.

For the use of the tool the following information is to be regarded:

- The first column "Number" should be consecutively numbered starting with 1 at the stack inlet and at the stack outlet each.
- The ground points, which could be sensors, pumps, valves or other conductive parts, are marked with an "x" in the column "grounded". They can be added and removed to review the effect of individual ground points.
- Precursors are important to allow correct calculation of the network. If the precursor is not given correctly, the calculation is likely not either.
- The segment description has no effect on the calculation but helps to remember which element is what segment in the 3D.
- When inserting new rows, the correct references have to be checked. If the references are not correct, part of the calculations will fail.
- The input fields "Length" and "Cross section" should be given according to the 3D data.

Project name		Demonstration		
Parameter name	Value	Unit	Note	
Reference conductivity @Tmax (stack outlet)	5	µS/cm	can be target or measurement, Tmax=80 °C	

Inputs

Outputs

AVL

Calculation of the isolation resistance via the coolant loop of a fuel cell system

Number	grounded[1]	Precursors[2]	Segment description	Length in mm	Cross section in mm2	Coolant conductivity in µS/cm	Isolation resistance in kOhm
			Stack inlet				660,83
1			Stack inlet interface stack 1	10,00	1000	5,0	20
2		1	MSU channels stack 1	150,00	800	5,0	375
3			Stack inlet interface stack 2	10,00	1000	5,0	20
4		3	MSU channels stack 2	150,00	800	5,0	375
5		2, 4	Pipe towards pressure sensor	156,00	1200	5,0	260
6	x	5	Pipe towards temperature sensor	400,00	1200	5,0	667
						5,0	
						5,0	
						5,0	
						5,0	
						5,0	
						5,0	
			Stack outlet				613,73
1			Stack outlet stack 1	50,00	1500	5,0	66,67
2		1	MSU channels stack 1	20,00	1000	5,0	40,00
3		2	MSU stack 1 until z_TCxStackOutl1	45,00	800	5,0	112,50
4		3	MSU channels stack 1	115,00	800	5,0	287,50
5			Stack outlet stack 2	50,00	1500	5,0	66,67
6		5	MSU channels stack 2	20,00	1000	5,0	40,00
7		6	MSU stack 2 until z_TCxStackOutl2	45,00	800	5,0	112,50
8		7	MSU channels stack 2	115,00	800	5,0	287,50
9		4, 8	interface MSU to piping	45	1000	5,0	90,00
10	x	9	pipe towards 3/2 way valve	680,00	1000	5,0	1 360,00
11	x	9	Pipe towards TCooltStackOutl	200	100	5,0	4 000,00
12	x	9	Pipe towards radiator	1000	1200	5,0	1 666,67
Total isolation resistance in kOhm							**318,21**

[1] at the end of the segment

[2] if more than one separate with comma (,); max 4

Version 1, May 2024

Figure 6-2: Layout of the isolation resistance calculator for the use

The detailed layout from Figure 6-3 is used for further descriptions and references to specific columns. The columns I:AC are defined as the calculation table. The columns do not contain inputs or outputs but can be viewed to deeper understand or adapt the model.

	A	B	C	D	E	F	G	H	I	J-Q (Precursors P1-P4 / successors S1-S4)	R	S-W (Ground Correction)	X-AA (Inputs)	AB	AC
8	Number	grounded 1	Precursors 2	Segment description	Length in mm	Cross section in mm2	Coolant conductivity y in µS/cm	Isolation resistance in kOhm	Calculation table -->	Precursors / successors	Ground Correction		Inputs	Output	Output Inverse
9										P1 P2 P3 P4 S1 S2 S3 S4	Number found in row x	G(P1) G(P2) G(P3) G(P4) Corrected Ground	I1 I2 I3 I4		

Stack inlet — Isolation resistance in kOhm: 198

Num	grounded	Precursors	Description	Length	Cross	y	Iso res	P1	S1	Num found	G(P1)	Inputs	Output	Output Inv
1			Stack inlet interface stack 1	10,00	1000	5,0	20		2	2	0	375	395	0,0025
2		1	MSU channels stack 1	150,00	800	5,0	375	1	5	5	0 x x	927	375	0,0027
3			Stack inlet interface stack 2	10,00	1000	5,0	20		4	4	0	375	395	0,0025
4	x	3	MSU channels stack 2	150,00	800	5,0	375	3	5	5	0 x x	927	375	0,0027
5		2, 4	Pipe towards pressure sensor	156,00	1200	5,0	260	2 4	6	6	0	667	927	0,0011
6		5	Pipe towards temperature sensor	400,00	1200	5,0	667	5		#NV		667	667	0,0015
						5,0				#NV			#VERT!	#VERT!
						5,0				#NV			#VERT!	#VERT!
						5,0				#NV			#VERT!	#VERT!
						5,0				#NV			#VERT!	#VERT!
						5,0				#NV			#VERT!	#VERT!
						5,0				#NV			#VERT!	#VERT!

Stack outlet — Isolation resistance in kOhm: 614

Num	grounded	Precursors	Description	Length	Cross	y	Iso res	P1	S1	Num found	G	Inputs	Output	Output Inv
1			Stack outlet stack 1	50,00	1500	5,0	67		2	2	0	1161	1227	0,0008
2		1	MSU channels stack 1	20,00	1000	5,0	40	1	3	3	0	1121	1161	0,0009
3		2	MSU stack 1 until z_TCxStackOutl1	45,00	800	5,0	113	2	4	4	0	1008	1121	0,0009
4		3	MSU channels stack 1	115,00	800	5,0	288	3	9	9	0 0	721	1008	0,0010
5			Stack outlet stack 2	50,00	1500	5,0	67		6	6	0	1161	1227	0,0008
6		5	MSU channels stack 2	20,00	1000	5,0	40	5	7	7	0	1121	1161	0,0009
7		6	MSU stack 2 until z_TCxStackOutl2	45,00	800	5,0	113	6	8	8	0	1008	1121	0,0009
8		7	MSU channels stack 2	115,00	800	5,0	288	7	9	9	0 0	721	1008	0,0010
9		4, 8	interface MSU to piping	45	1000	5,0	90	4 8	10 11 12	10	0	1360 4000 1667	721	0,0014
10	x	9	pipe towards 3/2 way valve	680,00	1000	5,0	1360	9		#NV	x	1360	0,0007
11	x	9	Pipe towards TCooltStackOutl	200	100	5,0	4 000	9		#NV	x	4000	0,0003
12	x	9	Pipe towards radiator	1000	1200	5,0	1667	9		#NV	x	1667	0,0006

Total isolation resistance in kOhm: 149

1 at the end of the segment
2 if more than one separate with comma (,); max 4

Version 1, May 2024

| Iso_Calc_FCS | Conductivity_Analysis | ⊕ |

Figure 6-3: Detailed layout for the isolation resistance calculator including the calculation table

6.1.3   Features

In this section the individual features and the specific implementation in Excel are discussed. Intentionally, macros are not used as the handling is more challenging and the servicing of the tool is more difficult.

6.1.3.1   Separation of Precursors

The input is given separated with a comma in column C to keep the input sheet lean. Therefore, it is necessary to separate the numbers and change the format to allow for calculations. The separation is done with the function *TEXTSPLIT* (German: *TEXTTEILEN*). For the conversion from text format to numeric format the function *VALUE* (German: *WERT*) is used. The precursor matrix from column J to M is the output of this function.

6.1.3.2   Definition of Successors

For the calculation of the isolation resistance the path from ground to the stack is followed. Therefore, it is essential to know not only the precursors but also the successors. The implementation is done with the Excel function *FILTER*. The matrix which shall be filtered is the column with the initial numbers (A). The filter rules are that the number of the row needs to be in the matrix of the precursors. Then, as the number shown has the number of the selected row as a precursor, it thus is a successor. As the filtered table is given as one column it is transposed into a row with the function *MTRANS*. The successor matrix from column N to Q is the output of this function.

6.1.3.3   Grounded Point Correction

There may be the case at which the ground points are put incorrectly leading to false calculation results. Therefore, a correction is implemented.

Figure 6-4 shows an example at which the labeling may lead to issues. In this case after R4 there is a ground connection. However, also R2 is grounded. If in the input sheet only R4 is labeled with "grounded" the ground check would identify a missing ground and add the ground connection to R2 too.
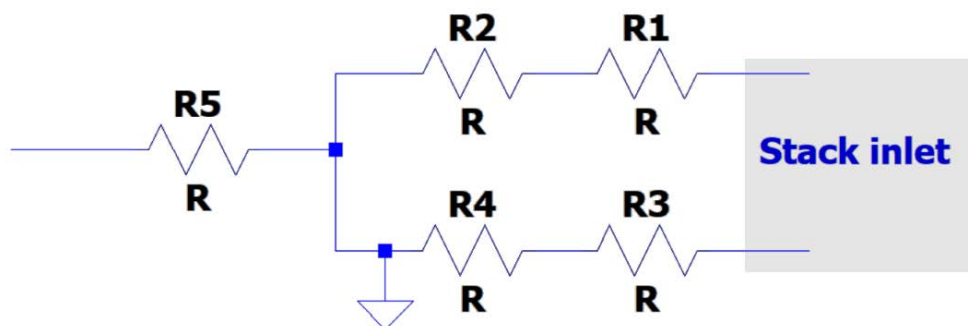
Figure 6-4: Example for potentially wrong grounded labeling

If R5 was grounded too, in Figure 6-4, it would not have an influence on the isolation resistance as only the first grounded point is relevant.

The process for the ground correction is displayed in a flow chart in Figure 6-5. It starts with a first step of searching for the segment number within the precursor matrix J:M. The result is shown in column R which is titled with "number found in row x". The function *XMATCH* (German: *VERGLEICH*) is used: It searches in a range and returns the position. The output is the row number in which the segment number was found within the precursor matrix.

In a second step the row where the segment number was found within the precursors, is searched for other precursors. If the precursor is grounded a "x" is the output. If either there is no precursor or it is not grounded the results nothing ("") or zero. The output is a matrix (S:V) to keep the function lean. In the matrix each column of the precursor matrix is transferred into the ground correction matrix. The implementation is done with a combination of the functions *VLOOKUP* (German: *SVERWEIS*) and *INDEX*.

The final result of the corrected ground uses the result of the ground correction matrix and further considers the ground input given by the user (as the ground correction matrix doesn't re-ground already grounded fields). Hence, if the segment number was grounded by the input, remains grounded. What the function cannot do is check whether the grounded points set in column B are correct or not. The output is an "x" indicating grounding in column W.
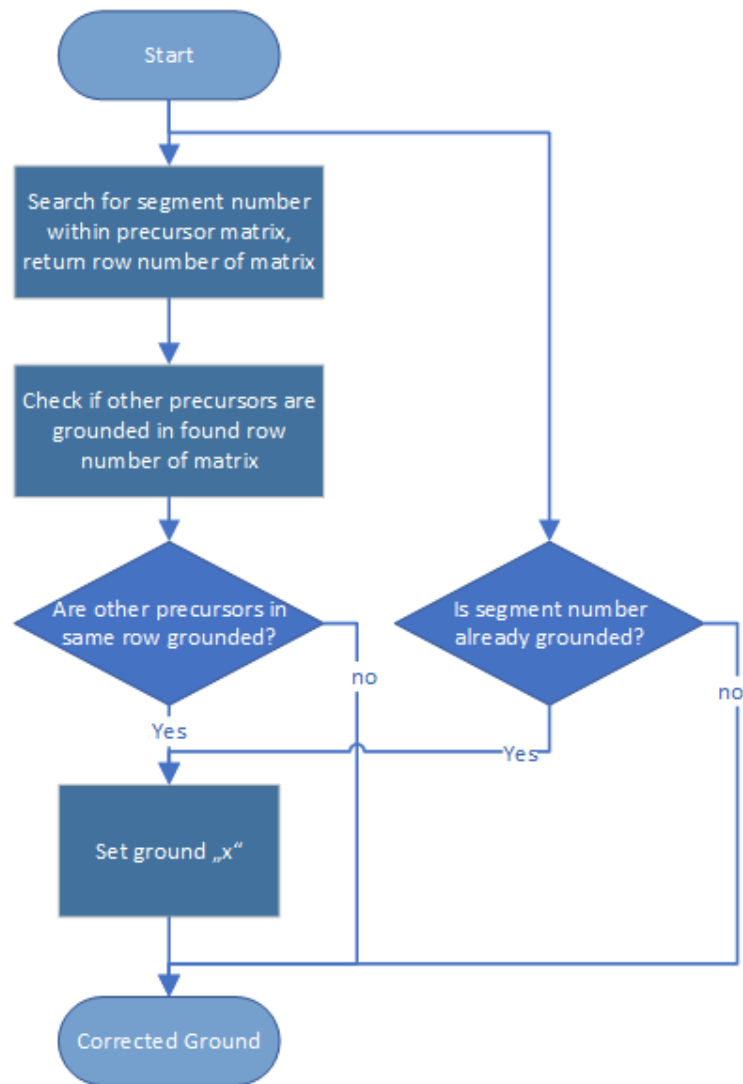
Figure 6-5: Flow chart for the ground correction function

6.1.3.4 Calculation of the Isolation Resistance

This feature can be considered the heart of the isolation resistance calculator. The calculation of the isolation resistance works from the grounded points backwards until the stack. For each segment, the isolation resistance output of the successor becomes an input. The calculation of the isolation resistance of a segment, implemented in column AB (see Figure 6-3) considers the following elements:

First, if the segment is grounded, the isolation resistance of the segment is the output. No inputs of the successors are considered. The relation is shown in equation (6-1).

$$Riso_{\text{out}} = Riso_{\text{seg}}$$

(6-1)

If there is no successor and the term is not grounded, the output is zero, as shown in equation (6-2)

$$Riso_{\text{out}} = 0$$

(6-2)

Otherwise, equation (6-3) is considered. Several successors indicate a parallel network according to equation (4-2) which is shown in the first term of equation (6-3).

$$Riso_{out} = \frac{1}{\frac{1}{In_1} + \frac{1}{In_2} + \frac{1}{In_3} + \frac{1}{In_4}} + Riso_{seg}$$

(6-3)

Where In_n is the **In**put assist column X:AA, it does not refer to a current value. For non-numeric In_n:

$\frac{1}{In} = 0$

Therefore, in case there is only one successor, equation (6-3) simplifies to

$$Riso_{out} = In_n + Riso_{seg}$$

(6-4)

Equation (6-4) then follows the rules of a serial resistance network as in equation (4-3).

6.2 Isolation Resistance and Conductivity Analysis

The aim of the isolation resistance and conductivity analysis sheet is to allow further quick judgements. The questions "What is the minimum isolation resistance per system to fulfill the requirements" and 'What is the highest allowed conductivity with the current grounded points while still fulfilling the legal isolation requirements?' shall be answered. The second question is answered with the information of the isolation resistance model and uses the conductivity as a variable.

6.2.1 Inputs and Outputs

The inputs and outputs of the conductivity analysis are shown in Figure 6-6. In that case the total isolation resistance at the reference conductivity given as the output in Figure 6-1 is an input into the model. To support the answer of the maximum allowed conductivity a plot showing the isolation resistance with the conductivity as a variable is created. For the judgement of the required isolation per FCS, the maximum voltage of the HV bus, the isolation requirement in Ω/Volt and the number of FCS which are intended to be in parallel are further inputs into the model.
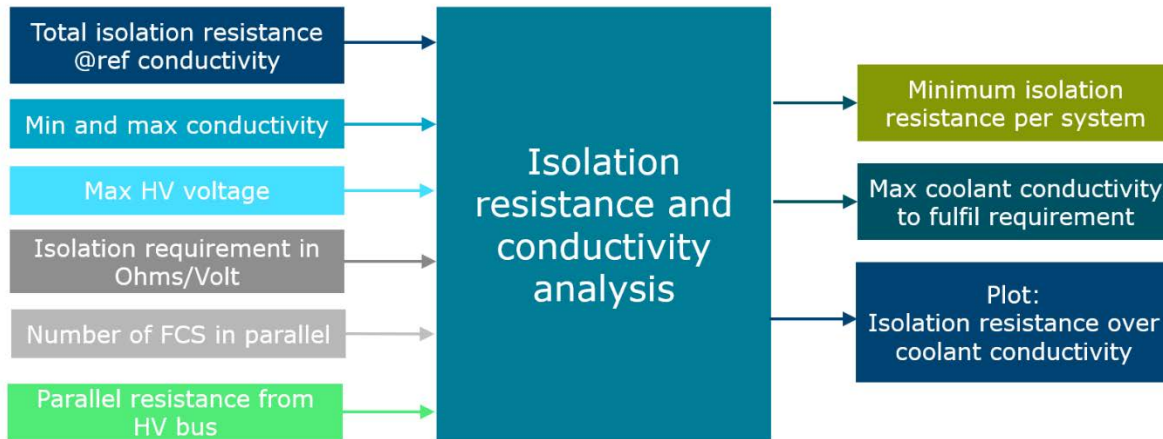
Figure 6-6: Inputs and outputs of the isolation resistance and conductivity analysis

6.2.2   Layout

The layout of the isolation resistance and conductivity analysis consists of an input box with yellow highlighted field indicating the required information.

Additionally, the reference conductivity is taken from the isolation resistance model sheet and analyzed whether it fulfills the requirements. Conditional formatting is set to indicate in red background if the requirements are not met and green background if they are. An additional text is written in the note field either stating "Reference conductivity is too high. RQ is not fulfilled" or "Reference conductivity fulfills RQ". RQ is the abbreviation for requirement.

The minimum isolation resistance per system as well as the maximum coolant conductivity to fulfil the requirement are highlighted with green background.

The plot shows the isolation resistance over the coolant conductivity where the grey line is the result of the minimum isolation resistance per system considering the input parameters. The blue line changes with coolant conductivity and is the result from the isolation resistance model. All values above the grey line are acceptable.

Parameter name	Value	Unit	Note
min. conductivity for x axis	1	µS/cm	
max. conductivity for x-axis	10	µS/cm	
Max. HV voltage	750	V	
RQ for isolation resistance	500	Ohms/V	usually 500 Ohms/V, in special cases 100 Ohms/V
Number of systems in parallel	1		increases the required isolation resistance per system
Additional parallel resistance from the HV bus	5000	kOhm	e.g. DCDC, battery, etc.
Reference conductivity @Tmax (stack outlet)	5	µS/cm	Reference conductivity is too high. RQ is not fulfilled

Minimum isolation resistance per fuel cell system[1]	405,41	kOhm
Maximum coolant conductivity	1,99	µS/cm
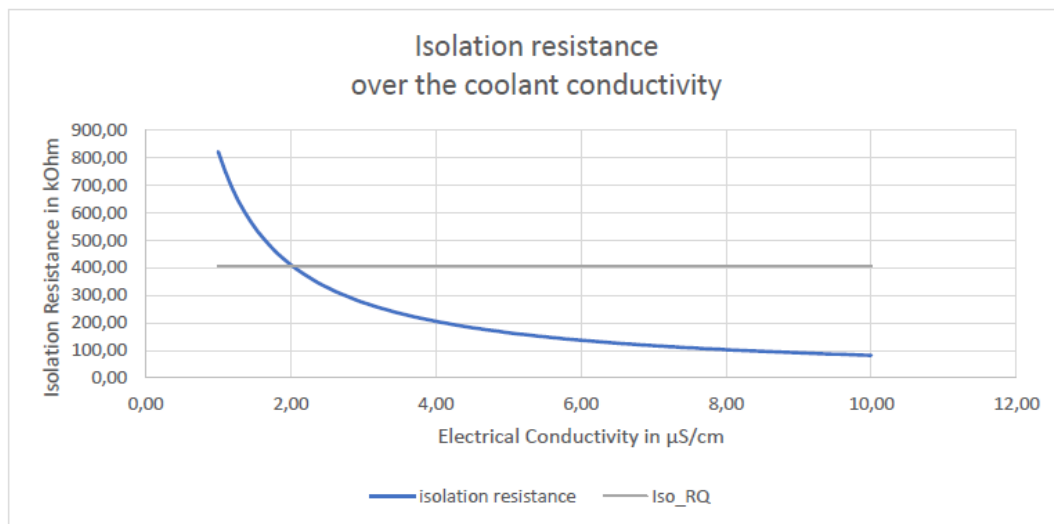
[1] only the coolant path, HV components like the compressor need to be considered in the parallel resistance of the HV bus

Figure 6-7: Layout of the isolation resistance and conductivity analysis

6.2.3   Features

This sheet consists of two features: the calculation of the minimum isolation resistance per FCS and the calculation of the maximum coolant conductivity. Both are explained in this chapter.

6.2.3.1   Calculation of the Minimum Isolation Resistance Per FCS

The minimum overall isolation resistance of the whole system $Riso_{min}$ is calculated with

$$R_{\text{iso min}} = Iso_{\text{RQ}} \cdot V_{\text{HV}}$$

(6-5)

Where Iso_{RQ} is the electrical isolation requirement in Ω/Volt and V_{HV} is the HV bus voltage in Volt.

Further, minimum overall isolation resistance can be calculated with

$$\frac{1}{R_{\text{iso min}}} = \frac{n}{R_{\text{iso FCS}}} + \frac{1}{R_{\text{iso HV}}}$$

(6-6)

Where n is the number of FCS, $R_{\text{iso FCS}}$ is the isolation resistance of one FCS and $R_{\text{iso HV}}$ is the isolation resistance of all other HV components.

Resulting in the final equation for the minimum isolation resistance of the fuel cell system $R_{\text{iso FCS}}$

$$R_{\text{iso FCS}} = n \cdot \frac{1}{\dfrac{1}{Iso_{\text{RQ}} * V_{\text{HV}}} - \dfrac{1}{R_{\text{iso HV}}}}$$

(6-7)

6.2.3.2 Calculation of the Maximum Coolant Conductivity

While in the isolation resistance model the isolation resistance is assessed only for the reference conductivity, the analysis of the maximum coolant conductivity requires a variation of conductivity.

The maximum coolant conductivity can be calculated with equation (6-8).

$$R_{\text{iso FCS}}(\sigma) = R_{\text{iso FCS}}(\sigma_{\text{ref}}) \cdot \frac{\sigma_{\text{ref}}}{\sigma}$$

(6-8)

Where $R_{\text{iso FCS}}(\sigma_{\text{ref}})$ is the isolation resistance of the FCS at the reference conductivity σ_{ref}.

7 Case Study AVL Fuel Cell Demo Truck

AVL has developed a fuel cell truck to demonstrate what aspects of fleet operator requirements need to be considered. In order to dissolve doubts about the practicality and integrability of fuel cell hybrid powertrains in existing truck platforms, a European 4x2 tractor with sleeper cab and a wheelbase of 3.8 m was chosen as the development basis. [34]

Figure 7-1: AVL HD Fuel Cell Technology Demonstrator Truck [34]

The high-level targets of the development are summarized in Table 7-1.

Table 7-1: Summary of high-level targets of AVL's Fuel Cell Demo Truck [34]

Truck targets	
Vehicle platform	European 4x2 semitrailer tractor with sleeping cabin and a wheelbase of 3.8 m
Vehicle gross weight	42 t gross combination weight
Driving range	> 400 km
Re-filling time H_2	< 15 min
Other	- Highway uphill driving without vehicle performance reduction in comparison to standard EU diesel trucks - No performance reduction up to ambient temperatures of 30°C (stretched target 35°C)
AVL developed powertrain systems	- Fuel cell system - E-axle - HV Battery system - H2 tank system - Vehicle thermal management system - Vehicle energy management system

A vehicle model was used to determine power requirements from real-life usage data as basis for the e-axle development. Furthermore, the optimized power split between fuel cell system(s) and HV battery was investigated to define the fuel cell system power as well as the HV battery power and capacity, also considering recuperation aspects. The comprehensive analysis revealed that the conversion of

conventional 40 t diesel-powered trucks toward fuel cell powered zero-emission powertrains requires 540 kW peak power at the axle and about 300 kW of fuel cell power to achieve competitive performance and cost. [34]

For the AVL Fuel Cell Demo Truck two fuel cell systems with a net power output of 156 kW at beginning of life are considered. Each fuel cell system includes a galvanically-connected boost DC/DC. The system size allows an optimal integration in the HV bus concerning the voltage level of e-axle, auxiliaries (including BoPs) and battery. The fuel cell systems operating voltage is from 410 V to 520 V. With a minimum voltage gap of 10 V which is required by the DC/DC from the low side to the high side the minimum HV bus voltage is 530 V. The maximum HV voltage is defined by the battery at 780 V.

With an HV bus voltage of 780 V and an isolation requirement of 500 Ω/Volt – as there is a combined DC and AC network – the minimum isolation resistance of the truck is 390 kΩ. With two fuel cell systems connected in parallel, the compliance becomes a challenge. Although the fuel cell system, more precisely the ground path via the coolant, is the biggest challenge with regard to isolation resistance it is not the only path to ground.

In the AVL Fuel Cell Demo Truck there are many HV components like inverters, compressors, pumps etc. An evaluation of their ground path resistances has been done based on the component specifications or development targets for AVL developed components. Based on the analysis of all components required in the truck, a budget of isolation resistance for each component was given. The required isolation resistance via the coolant for each FCS is 2 MΩ.

Within this chapter, the isolation resistance is first modelled and verified with measurement data and then, measures for improvements are suggested and classified by their effectiveness.

7.1 Isolation Resistance Model

During commissioning of the fuel cell system for the AVL Demo Truck at the test bed, the isolation resistance as well as the coolant conductivity are measured. Therefore, the isolation resistance model from chapter 6 is set up with the segmented 3D data of the coolant path, the grounded points and the reference conductivity of the AVL Demo Truck. The data is used to verify the model and to assess its accuracy.

The relevant grounded points are the following:

- Temperature sensor at the coolant stack inlet
- Pressure sensor at the coolant stack inlet
- Temperature sensor at the coolant stack outlet
- 3/2 way valve (from stack outlet)
- Radiator (from stack outlet)

The reference conductivity is chosen at 5 µS/cm. It provides a realistic view on expectable results, however, the choice of the reference conductivity is of minor importance. The conductivity analysis

provides the isolation resistance as an output in dependance of the coolant conductivity which then allows judgement what conductivity would be required to match the requirements.

To compare the results of the model with measurement data it is necessary to take the parallel resistances of the test bed into account. The relevant resistance paths are shown in Figure 7-2. The E Storage is the test bed load used acting as a battery simulator. The resistance values can be easily measured at the test bed if the stack is disconnected from the HV bus with open stack contactors while all other HV components are already connected. As long as the coolant is not filled the contactors can also be closed. Then the stack resistance to ground other than via the coolant can also be assessed.
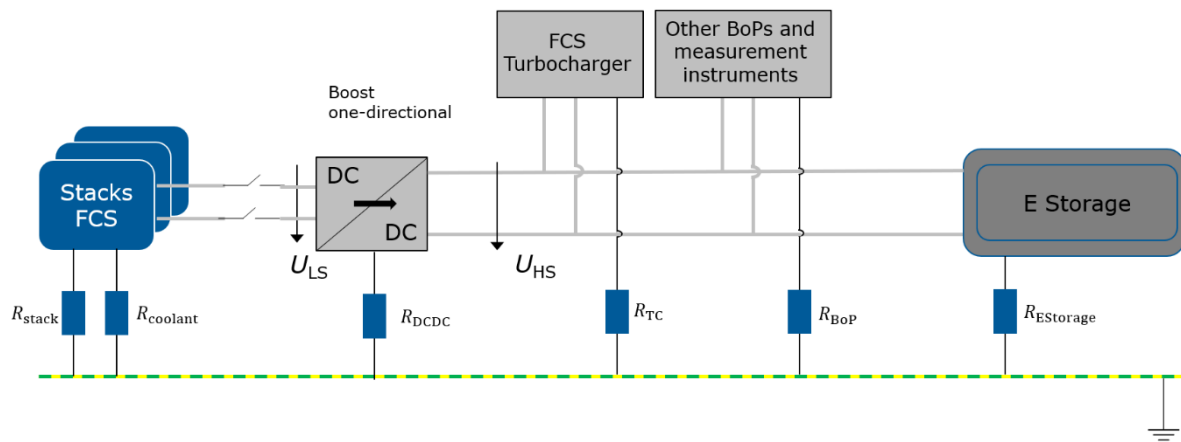
Figure 7-2: Resistance paths to ground from system and test bed

For the FCS of the AVL Demo Truck the measurement has been done stepwise to additionally assess the individual resistances. The total measured parallel resistance to ground at the test bed is 1.65 MΩ. The individual contributions are shown in Table 7-2. The measurement is crucial to understand the portion from the resistance to ground coming via the coolant circuit.

Table 7-2: Resistances to ground at the FCS test bed

Component	Value in kΩ
R_{stack}	10000
R_{DCDC}	50000
R_{TC}	50000
R_{BoP}	50000
$R_{EStorage}$	2200
Result	**1650**

Knowing the budget of 2000 kΩ for each FCS and the parallel resistance of 1650 kΩ at the test bed, the minimum isolation resistance of 900 kΩ can be calculated using equation (7-1). This value can directly be compared with the measurement results to judge whether the requirement is fulfilled.

$$\frac{1}{R_{iso\,min\,TB}} = \frac{1}{R_{iso\,min\,FCS}} + \frac{1}{R_{iso\,HV}}$$

(7-1)

Figure 7-3 shows modelled and measured data of the 156 kW FCS. The results are from the FCS test bed including the resistances from Table 7-2. The measured data points are colored according to their date of origin. Lighter points are from early measurement, the darker the point the later the data was measured. The analysis is done in AVL Data Analytics which is a big data analysis tool. The modeled data is included in the tool as a specification. The measured data is filtered for 20 seconds steady state points meaning the stack current was stable for at least 20 seconds for the shown points. As the output of the isolation resistance and the measurement window have a few seconds delay, dynamic points are not always shown correctly and are therefore excluded from this plot.
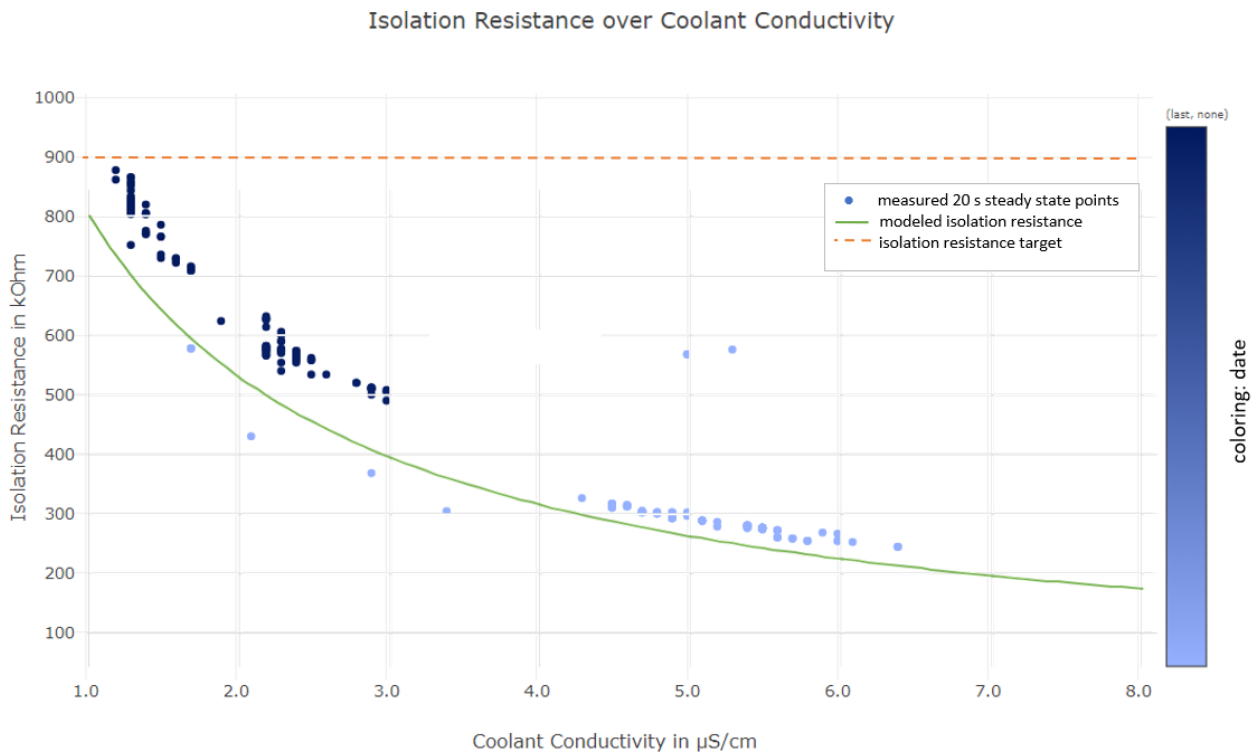
Figure 7-3: Isolation resistance at the FCS testbed over coolant conductivity, modelled vs. measured

One can see a wide spread of conductivity from the measurement points. During operation the conductivity changes with the temperature of the coolant see chapter 4.2.2.4. Further, it is typical that within the first operating hours the conductivity is not yet stable. Often, it initially rises before it gradually reduces and stabilizes.

For the validation of the model a wide spread of conductivity is helpful, which is why old and new data has been used in Figure 7-3. The offset between measurement data and modeled data is up to 20 %.

Generally, for lower conductivities the gap between modelled and measured data increases. In that range an inaccurate conductivity reading has quite a big effect. At the test bed the conductivity is measured at one point only, namely at the radiator inlet. At this point there is the highest temperature, therefore also the highest conductivity. While this temperature matches the stack outlet temperature well, therefore also models the stack outlet path to ground well, there is quite an offset for the stack inlet path to ground. During operation the delta temperature between inlet and outlet is load point dependent between 2 °C and 20 °C. To judge what that gap means in terms of conductivity, Figure 7-4 is used.

In Figure 7-4 exemplary stack inlet and stack outlet temperatures are marked, which could be rated power points. The difference in coolant conductivity for 19 °C temperature change is 25 %. This means for rated power the resistance path via the stack inlet is 25 % too low. Assuming the resistance via stack inlet and stack outlet is identical, that would lead to a 12.5 % too low isolation resistance model output. This, however, is only valid for rated power as the temperature difference at idle load point is only around 2 °C and for other load points somewhere in between.
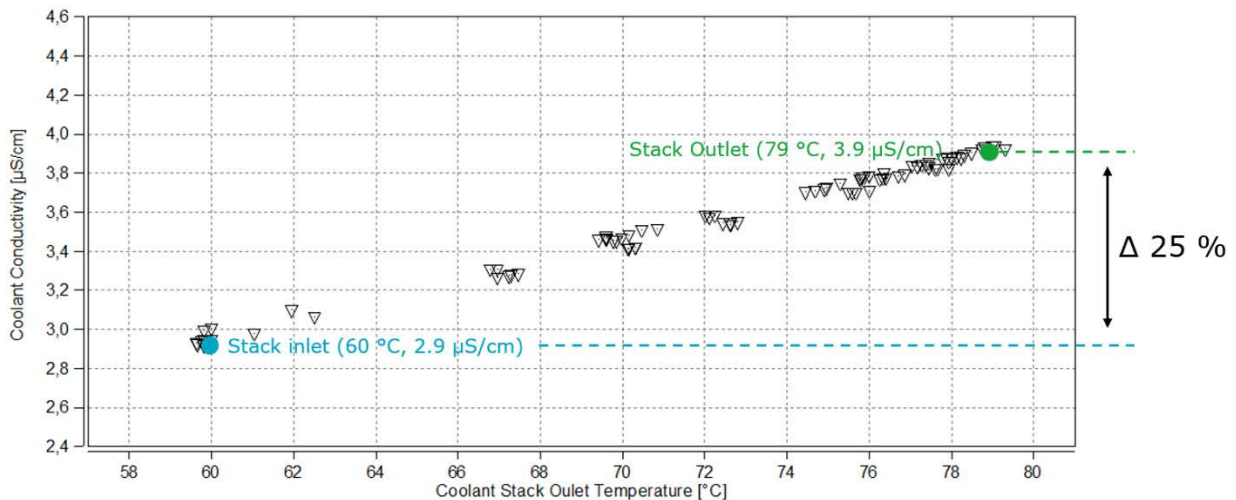
Figure 7-4: Coolant conductivity over the coolant stack outlet temperature

The model itself is not corrected by the temperature caused offset. It is favorable to show rather too low isolation resistances than too high ones. In the first case one would simply overachieve the targets while the second one would mean failing them which could have serious consequences for a project.

From the 20 % offset between measurement and model in Figure 7-3, 12.5 % can be attributed to the single point conductivity measurement, the temperature dependency of the coolant conductivity and the delta temperature during operation.

Other reasons for deviations between model and measurements can be:

- Deviation between 3D model and hardware, can lead to positive or negative offset.
- Accuracy of isolation monitoring device, typically 15 %. Usually, measurements show rather too low values than too high.
- Dynamic operation, can lead to positive or negative offset.
- Parallel resistances of the HV bus not correctly assessed, can lead to positive or negative offset.
- Low parallel resistance on the HV bus, meaning their influence gets bigger and measurement accuracy for the fuel cell system's isolation resistance reduces.

The results in Figure 7-3 further show that the target of 900 kΩ is not reached. Measures have to be taken to improve the isolation resistance via the coolant loop.

7.2 Measures

As the fuel cell system testbed target of 900 kΩ is not reached with the first design stage, measures need to be taken to further improve it. For the evaluation of measures the isolation resistance via the coolant is directly analyzed. The fuel cell system target is 2 MΩ per system.

To evaluate the effectiveness of the measures, the current design stage is taken as a reference. At a conductivity of 5 µS/cm the value is 302 kΩ.

7.2.1 Increasing Distance to Ground

The physical temperature sensors are eliminated and the pressure sensor is moved further away from the stack to increase the distance to ground.

1. **Implementation of vrtual sensors**

To increase the distance to the first grounded points the coolant inlet as well as the coolant outlet temperature sensors are eliminated according to chapter 5.4 and replaced by virtual sensors.

At the reference conductivity of 5 µS/cm the isolation resistance improves from 302 kΩ to 315 kΩ, which is around 4 %. Solely considering the isolation resistance this is not enough to justify such a measure. However, there is still the pressure sensor at the stack inlet as a first grounded point.

2. **Move pressure sensor further away from the stack**

The advantage with pressure sensors is that they can easily be moved to different positions, as long as there is no significant pressure loss in between. A small diameter pipe of approximately 500 mm is used as an extension from the main pipe to the sensor. This way the position can be changed without changing the existing piping.

At the reference conductivity of 5 µS/cm the improvement is from 302 kΩ to 357 kΩ. In this calculation the temperature sensors are still in place. This is already an improvement of approximately 15 %.

While both measures on their own only have little effect, their combination can significantly move the first grounded point and therefore improve the isolation resistance. The resulting isolation resistance with both measures is 414 kΩ, which is an improvement of 37 % compared to the reference. The result is shown in Figure 7-5.
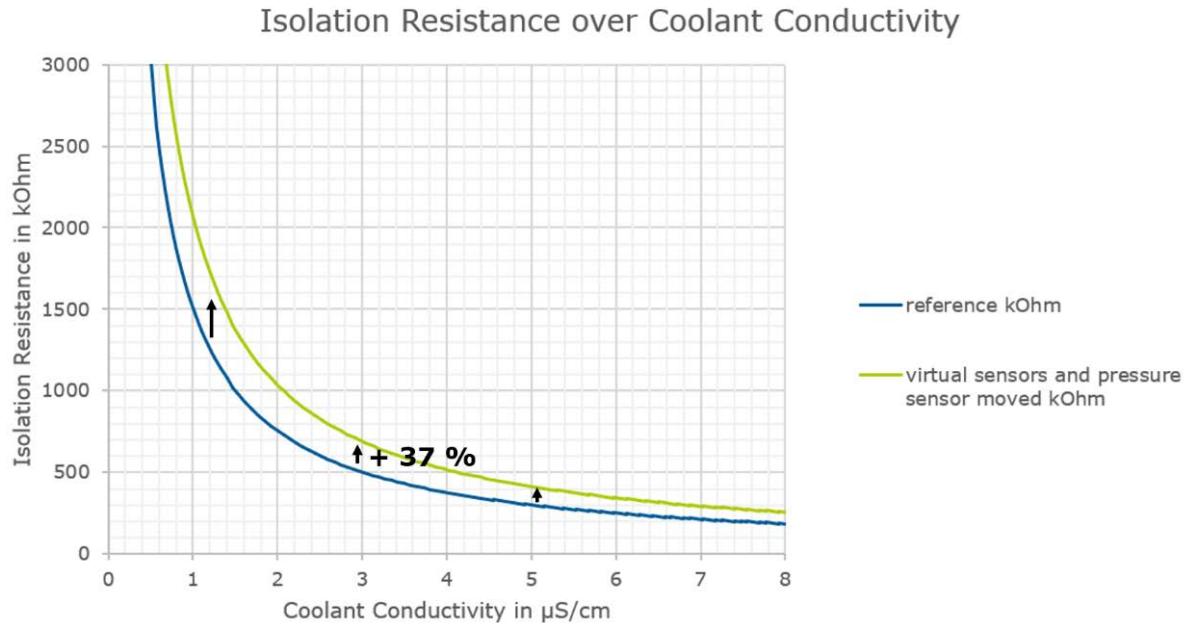
Figure 7-5: Modelled effect of measures to increase distance to ground on isolation resistance

7.2.2 Reducing Coolant Conductivity

With the implemented optimization measures from chapter 7.2.1, the target of 2 MΩ is reached at a coolant conductivity of approximately 1 µS/cm (see Figure 7-5). Although measurements from the test bed were in that range, with increasing temperature the limit was exceeded. Therefore, additional measures to reduce the coolant conductivity are taken.

1. Change coolant hose material

Tests to review different coolant hose materials were conducted.

For all hoses in Figure 7-6 the same coolant is used, except for the second measurement of the platinum cured silicone hoses from supplier 1, indicated in pink. Further, all hoses are tested with the same procedure: overnight hot conditioning, deionization and heat up. The curves are shown from the final heat up.

The FKM hoses from supplier 2 (in red) are the originally chosen hoses with which the data from Figure 7-3 is recorded. The intention is to change to a different material if the results show better results.

The results are difficult to analyze as they show contradictory results. The highest and the lowest result is from the same hose. The only difference is the coolant used. It is unclear, whether the coolant alone can have such a big influence on the result. More likely, there was an unintended contamination causing the first test result. Platinum cured silicone is known to result in low conductivities from other projects within AVL as well.

The low conductivity for the platinum cured hoses of supplier 1 could later be repeated in the chemistry lab in a simplified set up. A repetition of the tests at the material test bed could not be

done. Still, with the data available, the first result (in black) is not further considered. The platinum cured silicone hoses from supplier 1 are also very cost competitive. Therefore, the choice of material taken for the optimized FCS is the platinum cured silicone hose from supplier 1.

TWI	Conductivity	Conductivity	Conductivity	Conductivity
°C	µS/cm	µS/cm	µS/cm	µS/cm
25,024	2,033	1,521	0,190	0,092
69,946	4,929	3,832	0,655	0,313
44,921	2,896	2,312	0,465	0,222
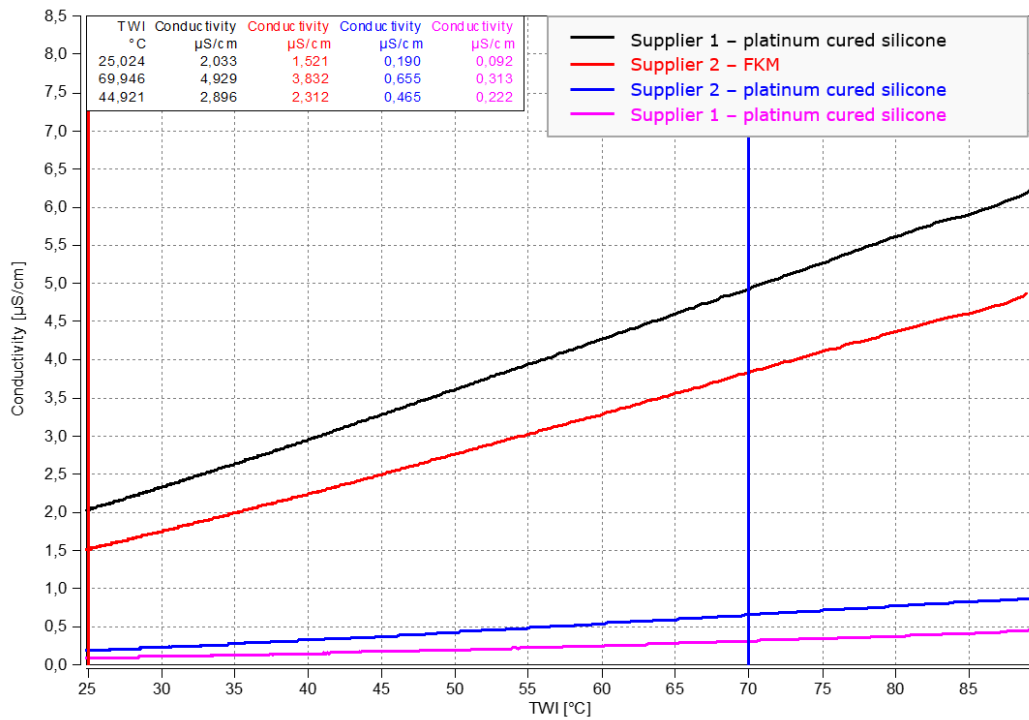
Figure 7-6: Deionization test at material test bed with 3 different coolant hose materials

2. Change coolant

For all coolants in Figure 7 6 the platinum cured silicone hoses from supplier 2 are used for the test Further, all coolants are tested with the same procedure: overnight hot conditioning, deionization and heat up. The curves shown are from the final heat up.

Although coolant 1 is only the second best coolant, it was chosen for the optimized FCS for the AVL Fuel Cell Demo Truck. It was earlier tested together with the selected coolant hoses which showed the excellent results. As the interactions between coolant and hose material are not yet fully understood, the already tested option with good results reduces the risks.
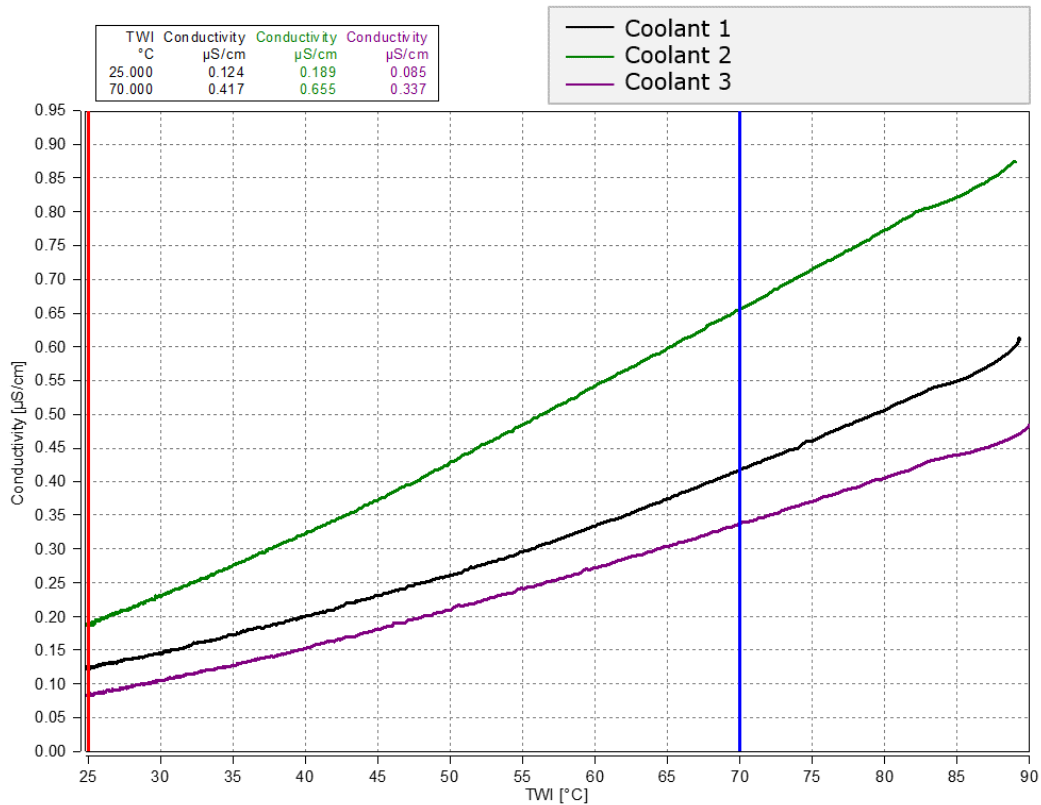
Figure 7-7: Deionization test at material test bed with 3 different coolants

If there are no other relevant sources of ions in the system, the expected coolant conductivity is below 1 µS/cm at all operating temperatures. It needs to be considered that this cannot be guaranteed for a prototype development such as the FCS for the AVL Demo Truck. Possibly, further optimizations followed by further tests have to be made. It is obvious that 1 µS/cm is a very ambitious target. Nevertheless, data from Demo Truck but also other systems at AVL show it is possible.

To sum up the results of the suggested measures a 37 % increase could be achieved from moving the grounded points and a further 400 % increase can be achieved by decreasing the coolant conductivity from 5 to 1 µS/cm. While the effect of reducing the coolant conductivity is much higher it needs to be considered that the outcome is much more unpredictable compared to the moving of the grounded points which is easily predictable with the created isolation resistance calculator of this thesis.

Improvement of isolation resistance via FCS coolant path of the FC Demo Truck

RISO via coolant	Reference @5µS/cm	Move ground point @5µS/cm	Decrease coolant conductivity to 1µS/cm
	302	414	2070

Isolation Resistance in kOhm

+ 37 %

+ 400 %
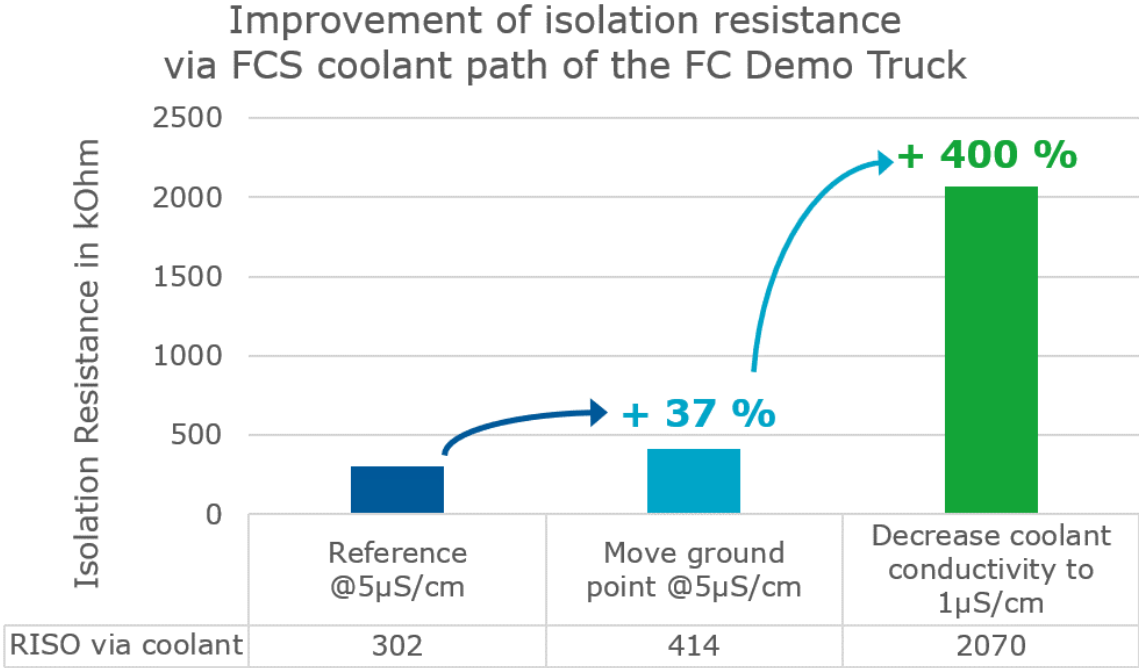
Figure 7-8: Evaluation of measures to increase the isolation resistance of the FCS for the Demo Truck

8 Discussion

As the main path to ground for the isolation resistance of a fuel cell system is the coolant path, it's isolation resistance can be modelled with the coolant conductivity and the 3D geometry of the coolant loop, at which length and cross section are the main parameters. The measures to improve the isolation resistance can be derived from the same relation. Precisely, the variables are: reducing the coolant conductivity, increasing the distance to ground and reducing the cross section of the pipe.

On the example of the case study AVL Fuel Cell Demo Truck the isolation resistance calculator was first used. Two fuel cell systems are electrically contacted in parallel on the HV bus of the truck. In the project, complying with isolation resistance requirements of 500 Ω/Volt is a challenge, which requires a combination of measures. Measures to reduce the maximum coolant conductivity from 5 to 1 µS/cm have the most significant effect. However, although material tests and other projects show the reduction is feasible it could not yet be achieved on the test bed for the fuel cell system of the Demo Truck. The risk related to relying on very low conductivities is high. Small contaminations can come from many sources: residues from production, degradation of the stack, corrosion, etc. The effort to reduce that risk like following a thorough cleaning procedure is high. To continuously allow operation of the fuel cell system in the vehicle, the isolation resistance must be sufficient at all time, even at end of life. As it is known that the coolant conductivity increases over time, low targets likely reduce the service interval and increase the risk of unplanned service stops.

One benefit of the isolation resistance model comes from knowing the maximum allowed conductivity. For fuel cell systems, the isolation resistance is not a value that is once validated at the at the end of line test to remain at the same level until end of life of the project. It is a challenge for all high-power fuel cell system automotive applications, and even beyond. Even if the targets are achieved at beginning of life, it is advantageous to know how much the conductivity is allowed to rise until the isolation requirements are violated.

While showing that meeting isolation resistance requirements is a challenge, the use case of the model could be well demonstrated. The offset of the model compared to the data analyzed is less than 20 %, which is sufficient for the use case. It is recommended to investigate the accuracy of the model for future projects as there are various variables that influence the accuracy of the measurements as well as the accuracy of the model. Therefore, a general statement on the accuracy cannot be given. It will be project-specific but with more data, the indication for the accuracy will still get better. For the data analyzed within this thesis, the model output shows a lower isolation resistance than the measurements, which is better than the other way around to avoid the system's isolation resistance is too low in the application.

As 12.5 % of the offset is linked to the temperature dependance of the coolant, the inputs of the model can be adapted to show an uneven conductivity distribution along the segments, especially between stack inlet and stack outlet. This can be done with the existing set up of the isolation resistance calculator. However, the results will then be valid for one load point only. The plot showing the isolation

resistance over the reference conductivity cannot be considered anymore. Due to those limitations the temperature compensation was not implemented in the model.

Again, referencing to the accuracy, the correct set up of the model is crucial. The geometry is usually easy to assess out of the 3D design. However, the version used needs to be up to date. Further, the grounding points are assessed for the model. A grounding concept is usually in place for the designed system. The concept sometimes is adapted at the testbed. Further, grounded test bed instruments are potentially added or removed during testing. The recommendation therefore is to set up the model as close to the testing phase as possible. That way the final model can be crosschecked directly with the hardware at the test bed.

A final recommendation is that for fuel cell system developments the isolation resistance target should be carefully chosen. The case study of the AVL Fuel Cell Demo Truck showed, that measures related to the grounded points can be well predicted but only have limited effect. Measures regarding the coolant conductivity have a significant effect but are hard to predict. Therefore, in some cases, the initial target isolation resistance may need to be reconsidered by optimizing the isolation resistance of other components of the vehicle.

References

[1]   United Nations Framework Convention on Climate Change, "The Paris Agreement - Publication," (Paris Climate Change Conference - November 2015), 2018.

[2]   H. Lee *et al.,* "IPCC, 2023: Climate Change 2023: Synthesis Report. Contribution of Working Groups I, II and III to the Sixth Assessment Report of the Intergovernmental Panel on Climate Change [Core Writing Team, H. Lee and J. Romero (eds.)]. IPCC, Geneva, Switzerland," 2023, doi: 10.59327/IPCC/AR6-9789291691647.

[3]   European Commission, "Regulation (EC) No 595/2009 of the European Parliament and of the Council of 18 June 2009 on type-approval of motor vehicles and engines with respect to emissions from heavy duty vehicles (Euro VI) and on access to vehicle repair and maintenance information and amending Regulation (EC) No 715/2007 and Directive 2007/46/EC and repealing Directives 80/1269/EEC, 2005/55/EC and 2005/78/EC," 2009. [Online]. Available: https://eur-lex.europa.eu/legal-content/EN/TXT/?uri=uriserv%3AOJ.L_.2009.188.01.0001.01.ENG&toc= OJ%3AL%3A2009%3A188%3ATOC

[4]   European Commission, "Regulation (EU) 2019/1242 of the European Parliament and of the Council of 20 June 2019 Setting CO2 Emission Performance Standards for New Heavy-Duty Vehicles and Amending Regulations (EC) No 595/2009 and (EU) 2018/956 of the European Parliament and of the Council and Council Directive 96/53/EC," 2019. [Online]. Available: https://eur-lex.europa.eu/legal-content/EN/TXT/?uri=CELEX%3A32019R1242

[5]   European Commission, "Proposal for a Regulation of the European Parliament and of the Council on type-approval of motor vehicles and engines and of systems, components and separate technical units intended for such vehicles, with respect to their emissions and battery durability (Euro 7) and repealing Regulations (EC) No 715/2007 and (EC) No 595/2009," 2022.

[6]   O. Gröger, H. A. Gasteiger, and J.-P. Suchsland, "Review—Electromobility: Batteries or Fuel Cells?," *J. Electrochem. Soc.*, vol. 162, no. 14, A2605-A2622, 2015. doi: 10.1149/2.0211514jes. [Online]. Available: https://iopscience.iop.org/article/10.1149/2.0211514jes

[7]   International Organization for Standardization, *Electrically propelled road vehicles — Safety specifications — Part 3: Electrical safety,* 4th ed. (ISO 6469-3:2021). London, UK: British Standards Institution, 2021.

[8]   International Electrotechnical Commission, *International Electrotechnical Vocabulary (IEV) - Part 212: Electrical insulating solids, liquids and gases,* 2nd ed. (International Standard IEC 60050-212:2010). Geneva, Switzerland: International Electrotechnical Commission, 2010.

[9]   International Electrotechnical Commission, *International Electrotechnical Vocabulary (IEV) - Part 195: Earthing and protection against electric shock,* 2nd ed. (International Standard IEC 60050-195:2021). Geneva, Switzerland: International Electrotechnical Commission, 2021.

[10]   International Electrotechnical Commission, *Effects of current on human beings and livestock,* 1st ed. (International Standard IEC 60479-1:2018). Geneva, Switzerland: International Electrotechnical Commission, 2018.

[11] H. Potdevin, "Insulation monitoring in high voltage systems for hybrid and electric vehicles," *ATZelektronik worldwide*, vol. 4, no. 6, pp. 28–31, 2009, doi: 10.1007/BF03242246.

[12] Sendyne Corp, "Safety of unearthed (IT) DC power systems," New York, 2019. Accessed: Oct. 6, 2023. [Online]. Available: https://www.sensata.com/sites/default/files/a/sensata-sendyne-safety-of-it-systems-whitepaper.pdf

[13] Bender GmbH & Co. KG, "ISOMETER® iso165C…: Insulation Monitoring Devices (IMD) for unearthed DC drive systems (IT systems) in electric vehicles," Datasheet, 2018. Accessed: Oct. 10, 2023. [Online]. Available: https://www.benderinc.com/fileadmin/content/Products/d/e/iso165Cx_D00154_D_XXEN.pdf

[14] T. E. Lipman and A. Z. Weber, *Fuel Cells and Hydrogen Production.* New York, NY: Springer New York, 2019.

[15] A. Tang, L. Crisci, L. Bonville, and J. Jankovic, "An overview of bipolar plates in proton exchange membrane fuel cells," *Journal of Renewable and Sustainable Energy*, vol. 13, no. 2, 2021, Art. no. 022701, doi: 10.1063/5.0031447.

[16] Q. Cheng, R. Zhang, Z. Shi, and J. Lin, "Review of common hydrogen storage tanks and current manufacturing methods for aluminium alloy tank liners," *International Journal of Lightweight Materials and Manufacture*, vol. 7, no. 2, pp. 269–284, 2024, doi: 10.1016/j.ijlmm.2023.08.002.

[17] T. Kiupel, "Best4Hy Deliverable D2.6: Report on the evaluation of MEA including recycled materials in PEMFC stack," 2024.

[18] G. Tsotridis, A. Pilenga, G. de Marco, and T. Malkow, *EU harmonised test protocols for PEMFC MEA testing in single cell configuration for automotive applications* (JRC science for policy report 27632). Luxembourg: Publications Office of the European Union, 2015.

[19] S. Smith and Bishop Mary, "Fuel Cell Coolants: Key characteristics of an effective coolant for fuel cell technology," Dober, 2023.

[20] A. de Frank Bruijn and G. J. M. Janssen, "PEM Fuel Cell Materials: Costs, Performance and Durability," in *Encyclopedia of Sustainability Science and Technology*, R. A. Meyers, Ed., New York, NY: Springer New York, 2017, pp. 1–41.

[21] International Organization for Standardization, *Electrically propelled road vehicles. Electrical specifications and tests for voltage class B systems and components,* 1st ed. (ISO 21498-1:2021). London, UK: British Standards Institution, 2021.

[22] *Electrical/electronic components in motor vehicles: Electrical properties and electrical safety of highvoltage components in motor vehicles: Requirements and tests,* BMW AG.

[23] J. Wu *et al.,* "A review of PEM fuel cell durability: Degradation mechanisms and mitigation strategies," *Journal of Power Sources*, vol. 184, no. 1, pp. 104–119, 2008, doi: 10.1016/j.jpowsour.2008.06.006.

[24] T. E. Burye, "Effect of PEM fuel cell exhaust water conductivity on catalyst degradation using thermal degradation resistant polymer membranes," *International Journal of Hydrogen Energy*, vol. 45, no. 20, pp. 11733–11748, 2020, doi: 10.1016/j.ijhydene.2019.11.232.

[25] B. Shantheyanda, S. Dutta, K. Coscia, and D. Schiemer, "Low Electrical Conductivity Liquid Coolants for Electronics Cooling," Dynalene, 2019. Accessed: Mar. 7, 2024. [Online]. Available:

https://www.dynalene.com/wp-content/uploads/2019/01/Low-Electrical-Conductivity-Liquid-Coolants-for-Electronics-Cooling.pdf

[26] I. Zakaria *et al.,* "A REVIEW OF NANOFLUID ADOPTION IN POLYMER ELECTROLYTE MEMBRANE (PEM) FUEL CELLS AS AN ALTERNATIVE COOLANT," *J. Mech. Eng. Sci.*, vol. 8, pp. 1351–1366, 2015, doi: 10.15282/jmes.8.2015.10.0132.

[27] Lenntech, "Dowex Ion Exchange Resins Fundamentals," 2000. Accessed: Apr. 15, 2024.

[28] M. H. Bargal, M. A. Abdelkareem, Q. Tao, J. Li, J. Shi, and Y. Wang, "Liquid cooling techniques in proton exchange membrane fuel cell stacks: A detailed survey," *Alexandria Engineering Journal*, vol. 59, no. 2, pp. 635–655, 2020, doi: 10.1016/j.aej.2020.02.005.

[29] R. Islam and B. Shabani, "Prediction of electrical conductivity of TiO2 water and ethylene glycol-based nanofluids for cooling application in low temperature PEM fuel cells," *Energy Procedia*, vol. 160, pp. 550–557, 2019, doi: 10.1016/j.egypro.2019.02.205.

[30] M. R. Islam, B. Shabani, and G. Rosengarten, "Electrical and Thermal Conductivities of 50/50 Water-ethylene Glycol Based TiO 2 Nanofluids to be Used as Coolants in PEM Fuel Cells," *Energy Procedia*, vol. 110, pp. 101–108, 2017, doi: 10.1016/j.egypro.2017.03.113.

[31] Arteco, "Freecor EV Micro 10: Datasheet," Accessed: Apr. 9, 2024.

[32] Dynalene, "Dynalene Ethylene Glycol Series: Engineering Guide," 2020. [Online]. Available: https://www.dynalene.com/wp-content/uploads/2020/05/Dynalene-EG-Engineering-Guide.pdf

[33] E. Ragonese, N. Spina, A. Parisi, and G. Palmisano, "An Experimental Comparison of Galvanically Isolated DC-DC Converters: Isolation Technology and Integration Approach," *Electronics*, vol. 10, no. 10, p. 1186, 2021, doi: 10.3390/electronics10101186.

[34] R. Döbereiner, J. Linderl, J. Pell, Rehrl, C. Schagerl, Steinek, R., and K. Weingrill, Eds. *Full Integration of a High-End Fuel Cell Powertrain into a European Long-Haul Tractor Unit*. Wien: Österreichischer Verein für Kraftfahrzeugtechnik (ÖVK), 2023.

Appendix

Table 1 shows the detailed reactions from current within different DC and AC zones (magnitude and duration). The DC and AC zones are shown in Figure 2-1 and Figure 2-2 respectively.

Table 1: Effects on human body for current zones of Figure 2-1 (DC) and Figure 2-2 (AC)

Range for AC	Range for DC	Effects on human body
AC-1	DC-1	No reaction
AC-2	DC-2	No harmful effects
AC-3	DC-3	Muscle contraction with reversible effects
AC-4	DC-4	Possible irreversible effects
AC-4.1	DC-4.1	Up to 5% probability of heart fibrillation
AC-4.2	DC-4.2	5–50% probability of heart fibrillation
AC-4.3	DC-4.3	Over 50% probability of heart fibrillation

Table 2 shows the voltage ranges according to GS 95023 with their operational and non-operational ranges.

Table 2: HV voltage ranges according to GS 95023 [22]

HV voltage ranges	HV operational status	Unit	HV_1	HV_2a	HV_2b	HV_3
Overvoltage at load dump[4]	B3 and B4	V pk	220	410	500	800
Upper HV electrical circuit limit voltage[4]	B3 and B4	V pk	220	410	500	800
Maximum operating voltage[3]	B2	V DC	200	360	470	770
Upper restricted operational capability[3]	B2	V DC	191 to 200	341 to 360	451 to 470	751 to 770
Unrestricted operational capability[3]	B1	V DC	90 to 190	170 to 340	250 to 450	520 to 750
Lower restricted operational capability[3]	B2	V DC	80 to 89	160 to 169	200 to 249	450 to 519
Highly restricted operational capability[3]	B2[1] B3[2]	V DC	60 to 79	120 to 159	150 to 199	-
Undervoltage[4]	B3	V DC	0 to 59	0 to 119	0 to 149	0 to 449

1) Components relevant for establishing readiness for driving.
2) Components not relevant for establishing readiness for driving.
3) Operating voltage ranges
4) Deviations from operating voltage ranges